

# Galactic polarization surveys

Wolfgang Reich<sup>1</sup>

Max-Planck-Institut für Radioastronomie  
Auf dem Hügel 69, D-53121 Bonn, Germany

July 22, 2018

<sup>1</sup>email:wreich@mpifr-bonn.mpg.de

# 1 Abstract

Following the detection of polarized diffuse Galactic emission in 1962 a number of surveys were undertaken at low frequencies in the following years resulting in important insights on the local magnetic field, polarization of the giant radio loops and other Galactic structures, as well as on the properties of the diffuse magnetized interstellar medium. This field of research experienced a revival in the eighties and nineties by a number of high resolution observations at low and high frequencies, which showed a large variety of polarization structures having no corresponding signature in the total intensity images. 'Canals' and 'Faraday screens' were reported, which clearly indicate that Faraday rotation in the magneto-ionic medium may largely vary on small scales. These findings called for a systematic approach and a number of new unbiased polarization surveys were started. Also new attempts for absolute calibration are under way, which is a critical issue when interpreting polarization structures. This paper reviews polarization survey projects and also summarizes recent results and interpretations of this rather active field of research.

# 2 Introduction

Galactic radio emission is made up from individual sources like supernova remnants (SNRs) or HII-regions, which are in their majority distributed along the Galactic plane and also from diffuse emission originating in the interstellar medium and extending towards high Galactic latitudes. Diffuse Galactic emission has a large volume filling factor and consists of synchrotron emission and the emission from ionized low density gas. Galactic radio sources are highly concentrated in the thin disk of the Galaxy and studies to derive their physical properties in most cases require high angular resolution observations for a wide range of radio frequencies. Polarization observations of synchrotron emitting sources like SNRs reveal information about the regularity of the magnetic field, its orientation within the object and also of the ambient interstellar field. Polarized radio emission suffers from Faraday rotation within the emitting volume and along the line-of-sight, which again requires multi-frequency observations to solve for that. All these effects are valid for diffuse emission as well, where the situation may be even more complicated by multiple emission layers along the line of sight, what requires to model the radiation transport conditions in some detail. Studies of the polarized diffuse Galactic emission received high interest during the last decade as Faraday rotation effects in the interstellar medium are thought to be responsible for a zoo of unusual polarized structures, which have no counterpart in total intensity. The analysis of polarized emission it is also expected to provide a deeper insight into the composition and structure of the components of the interstellar medium.

The basis for studies of Galactic polarized emission are large-scale surveys. These are time consuming projects and a number of surveys are actually running or planned to map and to analyse these puzzling phenomena in more detail. They are believed to provide some key information on Galactic magnetic field properties and also on weak thermal emission features. These investigations in some way complement polarization studies of nearby galaxies, which reveal the magnetic field structures on

scales of a few hundred parsec and larger, which are for obvious reasons much more difficult to perform for the Milky Way. A high interest in the polarized Galactic emission comes from groups aiming to study polarized fluctuations of the Cosmic Microwave Background (CMB) in the near future, where the weakness of the effect requires to take the Galactic foreground emission and its statistical properties into account.

### 3 History

After the detection of polarized emission from strong radio sources by Mayer et al. [1] subsequently also polarized emission from the diffuse Galactic emission was detected nearly simultaneously by Westerhout et al. [2] and Wielebinski et al. [3] at 408 MHz. Those observations finally established the synchrotron emission process as the major component of the diffuse Galactic emission at low radio frequencies. However, the percentage polarization of these observations was much lower than the theoretical maximum, which is close to 70% for a regular magnetic field. Faraday rotation originating within the interstellar magneto-ionic medium (MIM) distributed along the line of sight changes the direction of the original polarization angle, which is orientated along the electric field vector and orthogonal to the magnetic field direction. Faraday rotation also causes depolarization, which is rather significant at low frequencies. Due to the technical possibilities during the sixties observations of extended Galactic polarization were limited to low frequencies. Furthermore the large beamwidths of low frequency observations reduce the intensity of the observed polarized signal by vector averaging effects ('beam depolarization') in addition.

Following its detection in 1962 systematic surveys of diffuse Galactic emission were carried out for the northern and southern hemispheres. In the northern sky observations at Cambridge (7.5-m 'Würzburg Riese' dish) by Wielebinski & Shakeshaft [4] and at Leiden (Dwingeloo 25-m telescope) by Berkhuijsen & Brouw [5] gave the first insight into the distribution of polarized emission across the sky. The observing frequency of 408 MHz means a low angular resolution, which is about  $2^\circ$  for the Dwingeloo telescope and  $7.5^\circ$  for the Cambridge dish. Southern sky observations by Mathewson et al. [6] using the Parkes 64-m telescope had a higher angular resolution, but were severely undersampled. During the following years polarization surveys were extended towards higher frequencies, e.g. at 610 MHz by the group in Dwingeloo [7, 8] and at 1407 MHz by Bingham [9] for the northern sky. The southern sky was observed at 408 MHz and 620 MHz with some complementary data at 1410 MHz by Mathewson et al. [10].

It is important to note that the definition of the polarized intensity scale differed among the early observations. Berkhuijsen [11] made a thorough analysis of the scaling of all available polarization surveys at that time and calculated the correction factors relative to the definition adopted by the IAU in 1973, which is based on Stokes parameters.

## 4 Galactic synchrotron emission

The theory of the synchrotron emission process [e.g. 12] describes the radiation from high energy cosmic-ray electrons in a magnetic field. For a power law distribution of the energy of the cosmic-ray electrons it can be shown that the observed emission  $I(\nu)$  depends on the number of electrons in the emitting volume  $N_e$ , the magnetic field component perpendicular to the line of sight  $B_\perp$  and the electron energy power law index  $\gamma$ .

$$I(\nu) \sim N_e B_\perp^{(\gamma+1)/2} \nu^{-(\gamma-1)/2} \quad (1)$$

thus  $\gamma$  is directly related to the observed spectral index  $\alpha = -(\gamma - 1)/2$  for observed intensities. Extended emission is the main component of large-scale surveys and is usually quoted in units of brightness temperature  $T_b \sim \nu^\beta$ , where the spectral index  $\beta$  is related to  $\alpha$  by  $\beta = \alpha - 2$ .

The Galaxy hosts large-scale magnetic fields with a typical strength of a few  $\mu\text{G}$ . Relativistic cosmic-ray electrons with typical energies between several hundred MeV and a few GeV are required for measurable synchrotron emission in the radio range. Diffuse Galactic synchrotron emission dominates the sky at low frequencies. It is highly concentrated towards the Galactic plane, but also extends to high latitudes. For instance the high latitude minimum temperatures observed across the sky at 1.4 GHz are around 0.4 K  $T_b$ .

Discrete synchrotron emitting sources are mainly identified as the remnants from supernova explosions, which form either expanding shells or diffuse nebula powered by the wind of the neutron star left from the supernova event. The shells of SNRs harbour strong magnetic fields, which were swept up during their expansion. These shock fronts are commonly considered as the favourable sites for effective cosmic-ray acceleration. After these particle escape the shock they suffer energy losses mainly by synchrotron cooling, but their lifetime is long enough that they may diffuse far out off the plane reaching large heights of a kpc or more.

Synchrotron emission is highly polarized. The degree of polarization  $p$  depends on the energy spectral index of the cosmic-ray electrons and calculates to:  $p = (\gamma + 1)/(\gamma + 7/3)$ . For typical values of  $\gamma$  between 2 and 3 the intrinsic percentage polarization  $p_{\text{int}}$  calculates between 69% and 75%. These values are higher than those observed, which is due to depolarization effects (see Sect. 7.3) and also to the degree of regularity of the magnetic field. The total magnetic field consists of a random ( $B_{\text{ran}}$ ) and a regular component ( $B_{\text{reg}}$ ), which give the total field strength  $B_{\text{tot}} = (B_{\text{ran}}^2 + B_{\text{reg}}^2)^{1/2}$ . Without depolarization the measured degree of polarization  $p_{\text{obs}}$  calculates to  $p_{\text{obs}} = p_{\text{int}}(B_{\text{reg}}^2/B_{\text{tot}}^2)$ .

### 4.1 Radio continuum surveys

A number of all-sky radio continuum surveys exist in the frequency range up to 1.4 GHz with angular resolutions of 0°6 at best [13 and references therein]. Figure 1 shows the all-sky 1.4 GHz survey in total intensity. An additional large-scale survey is available at 2.3 GHz [14]. At higher frequencies (up to 10 GHz) ground based surveys were restricted to the narrow band of the Galactic plane, where higher angular resolutions are needed to resolve the complex emission structures (see Sect.

1420 MHz

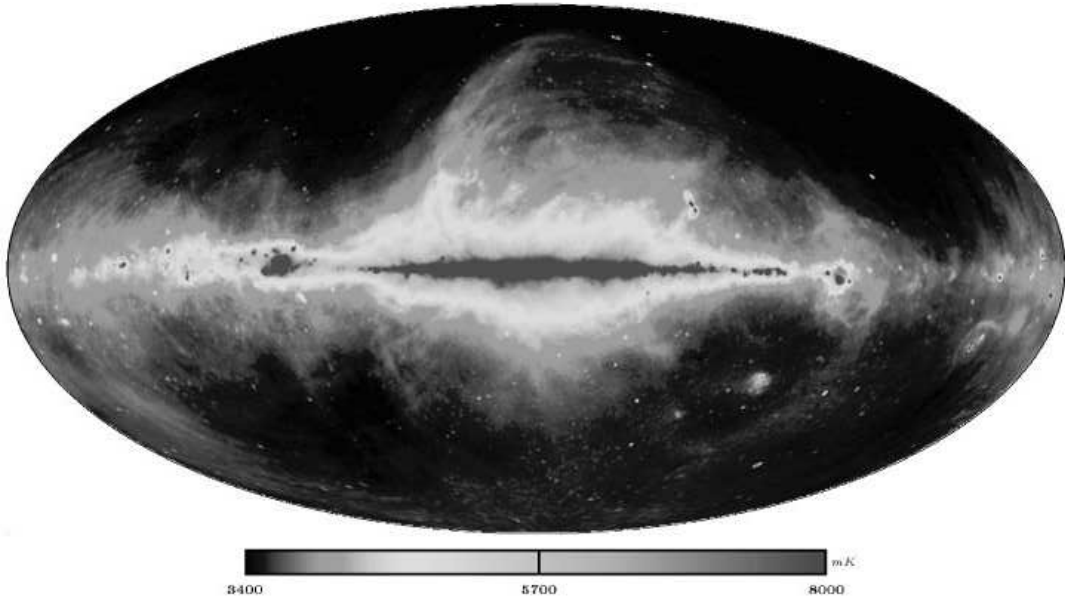


Figure 1: Absolutely calibrated 1420 MHz all-sky map in Galactic coordinates combined from northern sky data observed with the Stockert 25-m telescope (Bonn University/Germany) [17, 18] and the southern sky data observed with the Villa Elisa 30-m telescope (IAR/Argentina) [19]. The Galactic Centre is at the centre of the map. The combined all-sky map [20] includes the isotropic 2.73 K component from the cosmic microwave background.

6.4). Recently new possibilities were opened by high frequency observations from satellites, which complement ground based all-sky surveys limited at a few GHz. These new all-sky maps are from WMAP and cover the frequency range above 22.8 GHz [15] at angular resolutions of about  $0.5^\circ$  or better at the higher frequencies. A summary of early and more recent total intensity surveys was given by Wielebinski [16].

The absolute calibration of the high frequency data, which were carried out with parabolic antennas, is obtained by comparing the survey maps with low angular resolution sky-horn measurements, which are mostly restricted to scans at fixed declinations. At low frequencies the Galactic sky temperature is so high that an absolute calibration can be done by temperature standards.

The spectrum of the diffuse Galactic radio emission varies with frequency and sky position. At low frequencies the synchrotron emission clearly dominates, while at higher frequencies the increasing fraction of thermal emission in particular in the Galactic plane results in a flattening of the spectra. Synchrotron spectra are also not the same throughout the Galaxy, as they depend on the magnetic field strength and the cosmic-ray electron spectra, which are known to steepen towards higher energies. In general flatter spectra are seen at low frequencies.

## 4.2 The Galactic magnetic field

There are several methods to obtain information about the global structure of the Galactic magnetic field and the local field. Our position inside the Galaxy requires

models to get its global structure, of course, there is a strong guidance by results obtained for nearby galaxies, which can be studied either as face-on or edge-on objects giving information about the distribution of the disk fields or the field in the halo. Several reviews of the magnetic field structure in nearby normal galaxies are available [e.g. 21, 22].

Attempts to model the Galaxy were made by Beuermann et al. [23] and Phillipps et al. [24], who deconvolved the 408 MHz all-sky survey of Haslam et al. [25]. At 408 MHz synchrotron emission clearly dominates Galactic emission. The emissivity distribution in the Galaxy was obtained by assuming a regular magnetic field along a logarithmic spiral structure. The ratio of regular to random magnetic field of the best model fit was found to be about unity. Strong et al. [26] used a different method based on comparing  $\gamma$ -ray emissivity with synchrotron emission to get the magnetic field strength as a function of the Galacto-centric radius. A steady decrease from the inner Galaxy to larger radii was obtained. The magnetic field strength close to the Sun is about  $6\mu\text{G}$ . Similar results were derived by Berkhuijsen (private communication, see [16, Fig. 14 ]) assuming equipartition between magnetic field energy and cosmic-ray energy densities using emissivities from the Beuermann et al. model.

The direction of the local magnetic field was derived using rotation measures (RM) (see Sect. 5.2) of pulsars of known distance [27, 28, 29, 30]. The direction derived points towards the Cygnus region in the northern hemisphere and towards the Vela complex in the southern hemisphere, supporting the view of a general orientation of the magnetic field along the spiral arms with a pitch angle of a few degrees. The regular component of the local magnetic field is about  $1.4\mu\text{G}$ , just a small fraction of the total local field of about  $6\mu\text{G}$ . Also for more distant spiral arms the magnetic field direction can be derived using pulsar RM data. Han et al. [30] derived  $4.4\mu\text{G}$  for the regular magnetic field in the inner Norma arm, where the total field strength on average is about  $10\mu\text{G}$  [26].

Of high interest is the existence or non-existence of "magnetic field reversals", which are predicted under certain conditions by the dynamo theory (see [31] for a recent review). For nearby spiral galaxies indications for field reversals are very rare [21]. At present there is a common agreement on a field reversal between the local Orion arm and the Sagittarius arm at a distance of a few hundred parsec. For Galactic spiral arms at larger distances possibly more field reversals might exist. Because of limited data this is discussed controversial. Significantly larger RM data-sets are needed to decide on this important question.

## 5 The interstellar magneto-ionic medium

### 5.1 Thermal emission

Emission from gas clouds being ionized by the photons of OB-stars is referred to as thermal emission. These HII-regions are also optically visible depending on the amount of extinction by dust. Beside discrete gas complexes also a large amount of diffuse low density gas is present. HII-regions and diffuse gas are concentrated in the Galactic plane with a smaller scale height compared to synchrotron emission.

However, sensitive H $\alpha$  surveys reveal the existence of thermal gas also far out of the Galactic plane. Its excitation is not entirely clear yet. Optically-thin emission spectra, which are seen mostly at frequencies above a few hundred MHz, are flatter than typical synchrotron spectra. For this reason the fraction of thermal emission increases towards higher frequencies.

The dispersion measure (DM) from pulsar observations as measured by the time difference of the pulse arrival time at different frequencies is directly related to the column density of thermal electrons along the line of sight. Using independent pulsar distances, e.g. as determined by HI absorption measurements, the distribution of the thermal electron densities can be derived. On this basis the thermal electron distribution for the Galaxy was modeled by Taylor and Cordes [32] and Cordes and Lazio [33].

The warm ionized gas has typical temperatures of a few thousand Kelvin, but also cold low density thermal gas seems to exist, which preferably surrounds HII-regions as inferred from low-frequency absorption measurements [e.g. 34] or recombination line measurements [35]. Optical observations indicate an increase of the gas temperature with distance from the Galactic plane [36], which is also indicated for some edge-on galaxies [37].

## 5.2 Faraday rotation

The coexistence of magnetic fields and thermal gas in the interstellar medium results in Faraday rotation. The amount of Faraday rotation also called the 'Faraday depth' is (in the simplest case) equivalent to the rotation measure (RM), which is defined as the slope of the polarization angle  $\phi$  versus  $\lambda^2$ , and calculates for a line of sight L [pc]:

$$RM[\text{rad m}^{-2}] = 0.81 \int_L n_e[\text{cm}^{-3}] B_{\parallel}[\mu\text{G}] dL[\text{pc}] \quad (2)$$

with  $n_e$  being the thermal electron density and  $B_{\parallel}$  the magnetic field component along the line of sight. A detailed discussion of 'Faraday depth' related issues was recently made by Brentjens and de Bruyn [38].

RM is positive in case the magnetic field direction points towards the observer and vice versa. The amount of Faraday rotation depends on the observing wavelength, where the observed polarization angle  $\phi$  depends on the intrinsic polarization angle  $\phi_o$  and RM by  $\phi = \phi_o + \text{RM } \lambda^2$ . Observations at two frequencies need to be combined to calculate RM. However, there is an ambiguity in RM, which can be solved by adding observations at a third frequency. Narrow-band polarimetry around a certain frequency is the preferred observing technique as the beams are very similar, depolarization variations are small and therefore the emission originates from the same volume. However, the low signal-to-noise ratio of narrow-band polarimetry may limit the accuracy of the measurements, that small RM differences are not easy to measure. A new method called 'Faraday Rotation Measure Synthesis' was recently introduced [38], which allows to analyse contributions from multiple sources along the line of sight and improves the signal-to-noise ratio of narrow-band polarimetry. An application of this impressive new technique to multi-channel wide-field Westerbork polarization images was recently made for observations of the

Perseus cluster [39].

In the case of a uniform mixture of thermal emission and synchrotron emission the so called 'slab-model' [40] describes the observed emission as a function of frequency. However, the distribution of emission components in the interstellar medium is certainly less uniform. Emitting sources with internal and external Faraday rotation are observed through the diffuse magneto-ionic medium along the line of sight, where clouds, shells or bubbles with no or very little total intensity emission ('Faraday screens') are embedded.

## 6 Galactic polarization surveys

### 6.1 Observing technique

Galactic synchrotron emission is linearly polarized. This requires to measure the Stokes parameter U and Q, from which the polarized intensity PI and polarization angle  $\phi$  calculate as

$$PI = \sqrt{(U^2 + Q^2)} \quad (3)$$

$$\phi = 0.5 \operatorname{atan} (U/Q) \quad (4)$$

Early polarization measurements were made with single-dish telescopes using rotating crossed dipoles as feeds. The power difference between the dipoles was measured. Special care must be taken for the antenna pattern ellipticity [4]. Another method was to measure the cross-correlation between the two feed dipoles [2]. There are two possibilities to obtain a set of Stokes parameters from correlation. In case the feeds couple out linear polarization Stokes parameters I, Q and V are obtained after correlation and a 90° phase shift of one signal. Coupling out two circular polarization components gives Stokes I, Q and U after correlation, which is the preferred configuration to measure linear polarization needed for Galactic polarization work.

The feeds and their adjustment in the telescope are critical components for successful polarization measurements. At low frequencies dipoles are used and at higher frequencies corrugated waveguide feeds. A number of methods are used to change linear polarization components into circular components and various microwave components are used for this purpose.

Figure 2 shows, as an example, a 8-channel narrow-band IF-polarimeter and an additional broad-band channel attached to the L-band receiver at the Effelsberg 100-m telescope. It is used for 1.4 GHz and 1.7 GHz polarization observations and for RM determination. At other telescopes correlator backends have been installed which allow to measure simultaneously wide bands split into hundreds of narrow channels. Analysis of these polarization data cubes require new techniques as the already mentioned 'Faraday Rotation Measure Synthesis' [38], for instance. At frequencies of 5 GHz and higher analog IF-polarimeter with a bandwidth of several hundred MHz up to a few GHz are available for measurements of the usually very weak polarized signals at these frequencies. This is possible since depolarization across the band becomes less important at high frequencies (see Sect. 7.3).

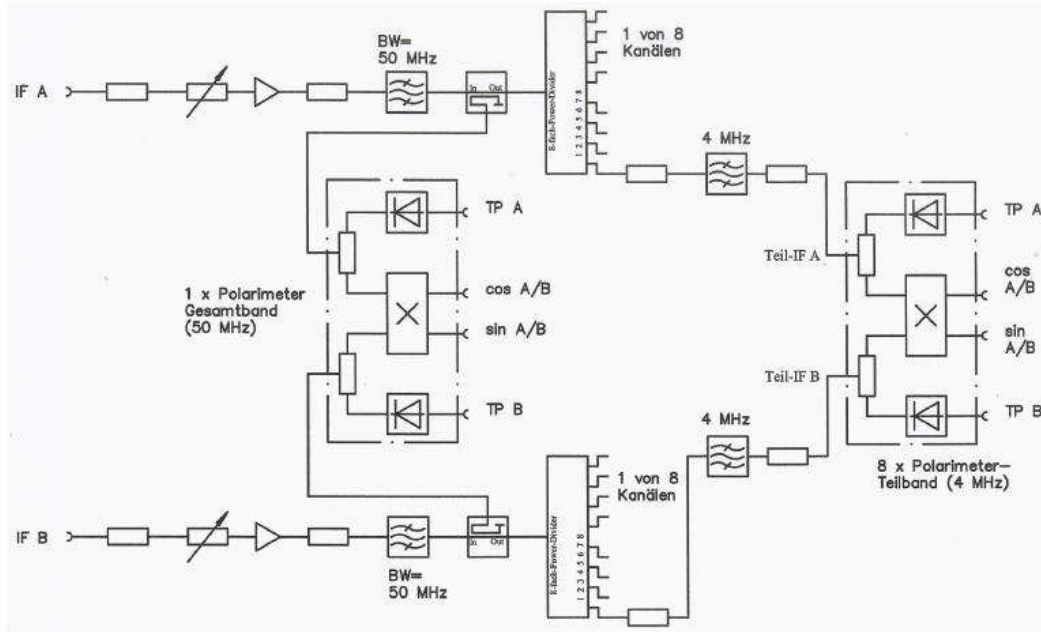


Figure 2: Block diagram of an IF-polarimeter with 8 narrow and one wide channel, which is attached to the L-band receiver installed at the Effelsberg 100-m telescope (courtesy of O. Lochner).

## 6.2 Instrumental effects

For polarization measurements a number of instrumental effects must be taken into account. The antenna feed and other frontend components cause losses or cross-talk between the polarization channels. The polarimeter response, in addition, may not be circular and the observed  $U$  and  $Q$  signals depend on the polarization angle or the parallactic angle for telescopes with an AZ-EL-mount. Instrumental effects may also vary with time. All these influences must be calibrated in a suitable way using measurements of unpolarized radio sources and an analysis of the polarized calibration signal to find the instrumental parameters. With the measured instrumental terms a  $4 \times 4$  correction matrix, the 'Mueller matrix', is set up, which simultaneously transforms the observed polarization components into the four Stokes parameters.

Sidelobes caused by strong polarized signals are similar in structure and level compared to the total intensity sidelobes. An example of a 6 cm polarization pattern is shown in Fig. 3. Unpolarized sources often show a 'butterfly'-shaped antenna response for the Stokes parameter  $U$  and  $Q$  in the area of the main beam. This causes a ring-like shaped characteristic for the polarized intensity response of an unpolarized source. Far-sidelobes are highly polarized and this may cause problems in particular for large-scale survey observations. The sidelobes pick up radiation from the ground and the observed sum of these spurious signals does not vary necessarily in a systematic way. In general ground radiation increases towards lower elevation often rather different in  $U$  and  $Q$ . An example for ground radiation profiles derived for the Villa Elisa 1.4 GHz polarization survey of the southern sky is shown in Fig. 4. Depending on the site of the telescope (e.g. mountains in the surroundings) the ground radiation may also vary with azimuth direction. The ce-

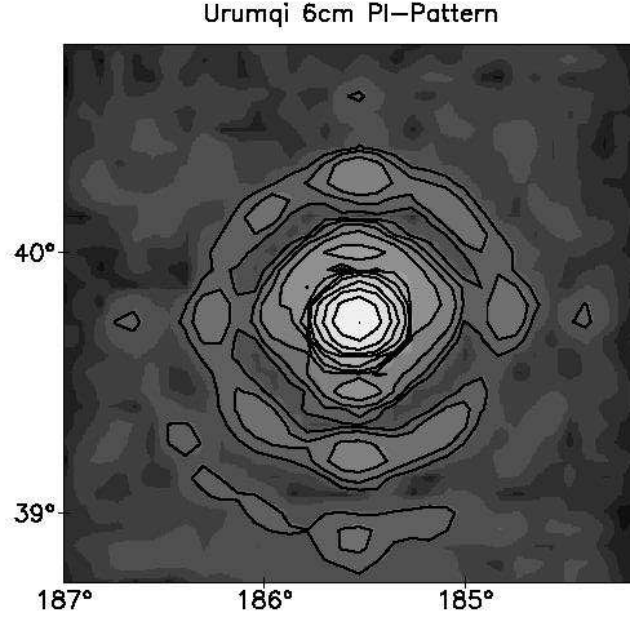


Figure 3: 6 cm antenna pattern for polarized intensities of the Urumqi 25-m telescope using the signal received from the INSAT-3B satellite. Contours run in steps of 3 dB down to -30 dB. The field size is  $2^{\circ}2' \times 2^{\circ}1'$ . The sidelobes are enhanced towards north, east, south and west due to the influence of the four telescope's support legs.

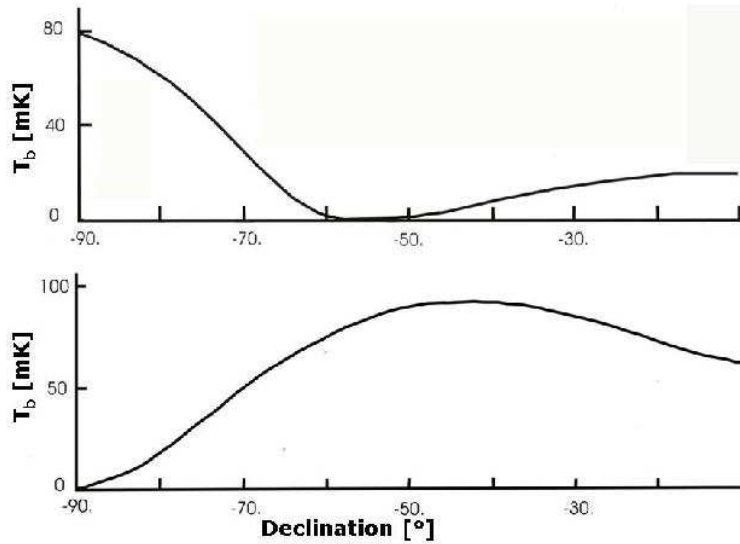


Figure 4: Ground radiation of the Villa Elisa 30-m telescope at 1.4 GHz. The profiles were derived from averaging a large number of scans along declination from various sky directions of the two polarimeter channels. The zenith for the Villa Elisa telescope corresponds to a declination of about  $-55^{\circ}15'$ . The intensity scale is in mK  $T_b$  with an arbitrary zero-level. [Testori et al., in prep.]

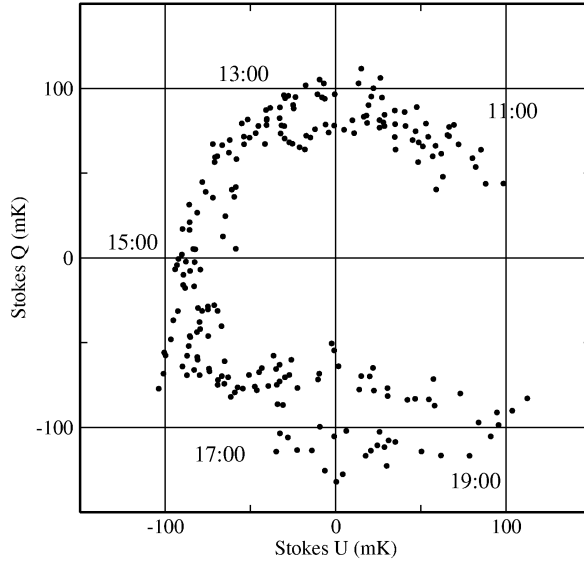


Figure 5: Example of an absolute polarization measurement (with preliminary calibration) towards the NCP at 1.4 GHz made with the 26-m DRAO telescope [43]. Apparent sky rotation causes a systematic variation of the signals in the 'U' and 'Q'-channel of the polarimeter with time (as indicated). Polarimeter offsets and the contribution from the ground are required to be constant during these measurements.

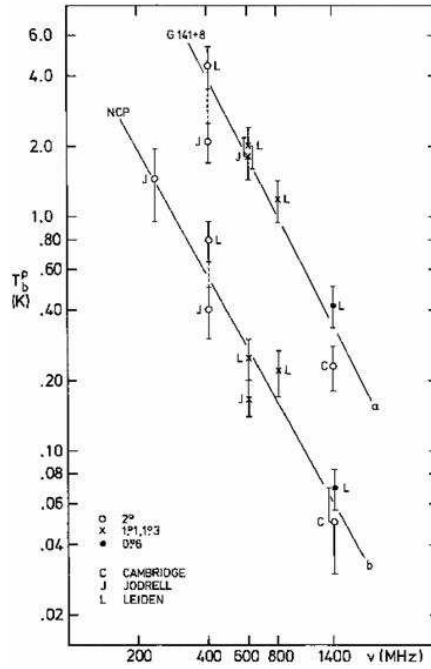


Figure 6: Low frequency polarization spectra towards the North Celestial Pole (NCP) and the calibration point at  $l, b = 141^\circ, 8^\circ$  [11]. The polarized intensity spectra are significantly flatter than those of the total intensity synchrotron emission. For the NCP data shown the spectral index is  $\beta = -1.8$ . Other NCP observations confirm the flat spectrum:  $\beta = -1.87 \pm 0.05$  [41] or  $\beta = -2.06 \pm 0.1$  [42].

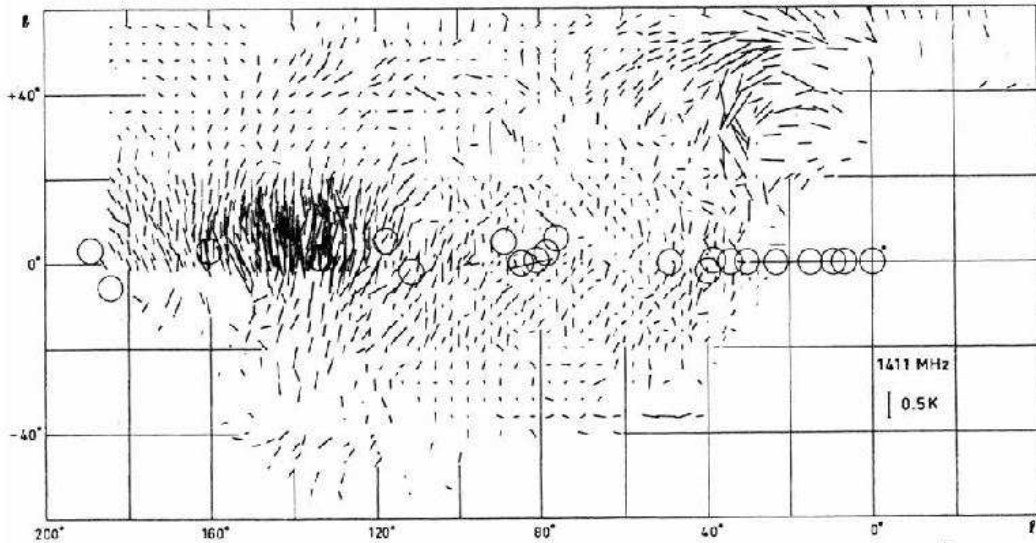


Figure 7: The Leiden-Dwingeloo 1.411 GHz polarization survey of the northern sky showing polarization bars proportional to polarized intensity in E-field direction [45].

lestial poles were often used for absolute polarization temperature measurements, because all instrumental contributions are (in principle) constant in this direction and by apparent sky rotation the polarization components describe a circle in the U,Q-plane as shown in Fig. 5, whose radius gives the polarized intensity. The low frequency spectrum for the North Celestial Pole is included in Fig. 6.

The far-sidelobe structure of a telescope depends on the reflecting or scattering support structures within the telescope [44]. Although the absolute level of the far-sidelobes is rather low (typically much below -50 dB) day time observations are often affected or become impossible due to scattered solar radiation picked up by the far-sidelobes.

### 6.3 Available large-scale surveys

A series of linear polarization surveys of the northern sky between 408 MHz and 1411 MHz were carried out using the 25-m Dwingeloo telescope and published in 1976 [45 and references therein]. All these surveys were on an absolute scale being corrected for the polarized ground radiation and also for Faraday rotation occurring in the ionosphere, which needs to be taken into account for frequencies below about 1.4 GHz. The angular resolution of these surveys varies according to the wide range of frequencies between  $2^\circ$  at 408 MHz and  $0.6^\circ$  at 1.411 GHz. The sky was not entirely mapped and the sampling was not complete. However, the data are available in numerical form and were widely used until today. Figure 7 shows the result of the 1.411 GHz survey in the form of polarization bars in E-field direction. Another series of polarization surveys were carried out with the Jodrell Bank 76-m telescope. A compilation of all large-scale northern and southern sky Galactic surveys published until 1976 is included in the paper by Spoelstra [46].

More recently several large areas of the sky were mapped with the Westerbork telescope at 327 MHz [47-50] and more work is in progress. These low frequency

## 1.4 GHz Polarized Intensity

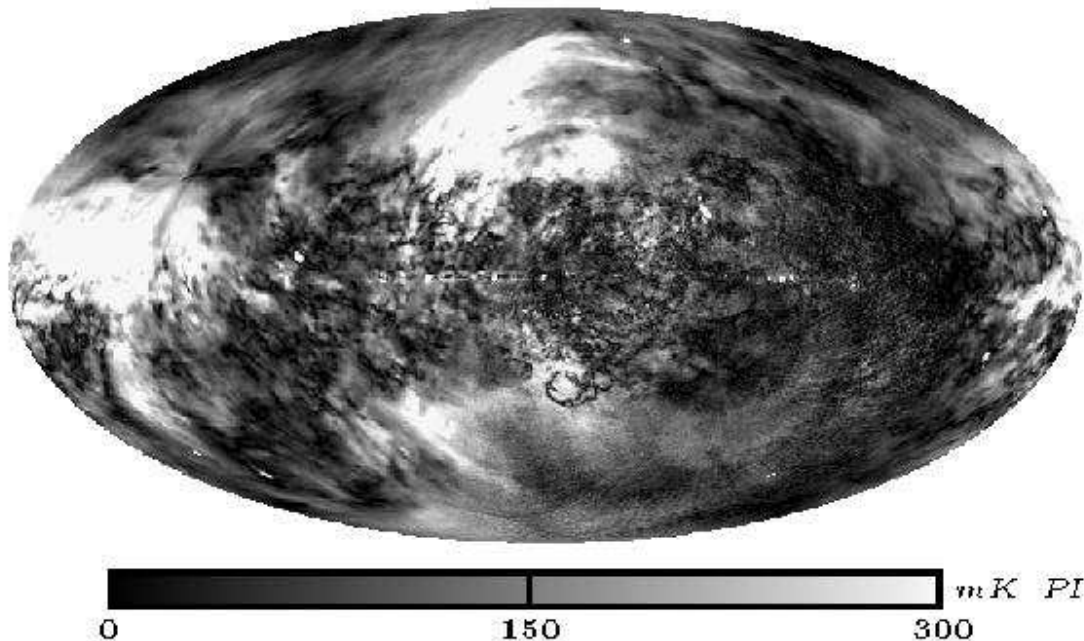


Figure 8: All-sky 1.4 GHz map in polarized intensity obtained by combining the northern sky polarization survey obtained with the DRAO 26-m telescope [56] and southern sky polarization data from the Villa Elisa 30-m telescope [58] after adjustment. The angular resolution of the map is  $36'$ , however, the northern sky data are not fully sampled in declination and thus were interpolated [56].

maps have arcminute angular resolution and reveal a wealth of small-scale polarization structures. The Westerbork observations were recorded in several narrow channels, what allows RM determination. The results of these observations have been interpreted in a series of papers [48-55].

As seen from Fig. 7 the Leiden-Dwingeloo northern sky survey at 1.411 GHz has no complete coverage and is also severely undersampled in large areas of the sky. A much more densely sampled new survey at 1.4 GHz was recently carried out using the 26-m telescope at the DRAO/Canada [56] at about the same angular resolution of  $36'$ , but five times higher sensitivity compared to the Leiden-Dwingeloo survey. The DRAO survey results from declination scans with the telescope's position fixed in the meridian. By apparent sky rotation fully sampled data along right ascension were obtained. In declination the sampling of the data varies between  $0^{\circ}25'$  and about  $2^{\circ}5'$  and therefore some interpolation is needed. The survey is described by Wolleben et al. [56], more details are given in [43, 57]. The DRAO data were tied to the absolutely calibrated Leiden-Dwingeloo data to find their temperature offsets. Polarization data from the Effelsberg 100-m telescope were used to fix the temperature scale. The data from the DRAO polarization survey are available at <http://www.mpifr-bonn.mpg.de/survey.html> (for selected fields in different projections) or at <http://www.drao.nrc.ca/26msurvey> or <http://www.mpifr-bonn.mpg.de/div/konti/26msurvey> (for the entire set of survey data).

Corresponding southern sky polarization data at 1.4 GHz will be also available

next time. They were observed with the Villa Elisa 30-m telescope simultaneously with the total intensity southern sky survey [19]. Some reduction procedures and first maps were already presented by Testori et al. [58]. Unfortunately no absolutely calibrated data are available for the southern sky so far. However, there is a large region of overlap between declination  $-10^\circ$  and  $-28^\circ$  with the DRAO northern sky survey, whose data are used to find the absolute polarization level for the southern sky. Villa Elisa maps of the strong, highly polarized and sufficiently extended radiogalaxy Centaurus A were used for scale and angle calibration in respect to maps from the Parkes 64-m telescope. A combination of the northern sky and the southern sky survey is shown in Fig. 8, which is the first all-sky polarization map obtained so far.

## 6.4 Galactic plane surveys

### 6.4.1 Radio continuum surveys

Radio continuum surveys of the Galactic plane need higher angular resolutions than all-sky surveys to resolve the large number of individual sources in the thin disk of the Galaxy from the diffuse emission, which is most intense in the Galactic plane as well. These surveys form the basis for detailed investigations of individual objects, but also for spectral investigations. Numerous surveys were made with single-dish telescopes. In particular the Effelsberg 100-m telescope was used for northern sky observations at 1.4 GHz [59, 60], 2.7 GHz [61, 62, 63] and at 4.9 GHz [64], where the angular resolution is about  $2'.6$ . The Parkes 64-m telescope was used for mapping the southern Galactic plane at 5 GHz with  $4'.1$  angular resolution [65]. 2.4 GHz Parkes maps were published by Duncan et al. [66]. The highest frequency Galactic plane survey comes from the Nobeyama 45-m telescope at 10 GHz with  $2'.7$  angular resolution [67].

Also synthesis telescopes were used to survey the Galactic plane, but they miss most of the diffuse emission and their maps of extended sources are often incomplete. Synthesis telescope surveys are, however, very well suited to measure compact sources in a complex environment. A combination of synthesis telescope surveys with single-dish surveys is needed to obtain maps including emission on all angular scales. This is for instance a standard procedure for the 408 MHz and 1420 MHz maps from the CGPS ('Canadian Galactic Plane Survey')[68], which are either combined with the 408 MHz all-sky survey [25] or the Effelsberg telescope surveys at 1.4 GHz [59, 60].

### 6.4.2 Polarization surveys

The Galactic plane survey at 2.7 GHz carried out with the Effelsberg 100-m telescope at  $4'.3$  angular resolution includes simultaneous observations of linear polarization [69]. The area between  $4^\circ.9$  and  $74^\circ$  Galactic longitude with a latitude range of  $\pm 5^\circ$  was complete in polarization [70]. The Parkes telescope maps at 2.4 GHz complement the Galactic plane in southern directions [71]. Some discussion and analysis of the properties of the polarized emission along the Galactic plane was made by Duncan et al. [70]. A section of the Effelsberg 2.7 GHz survey is shown

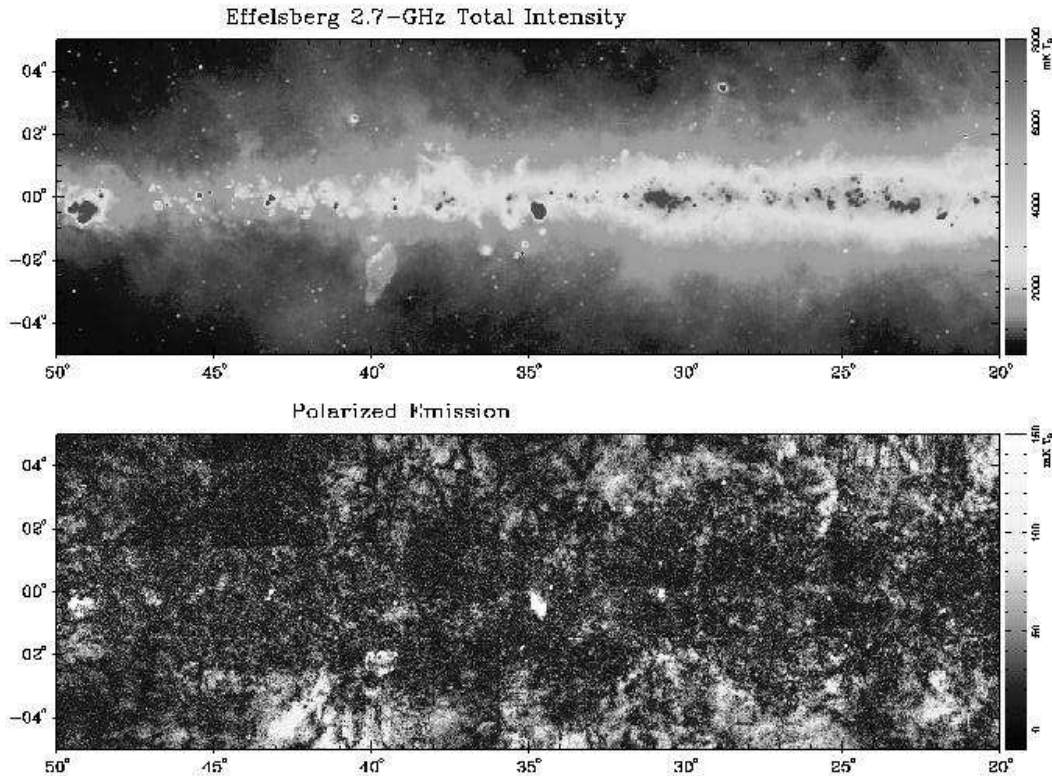


Figure 9: Section of the 2.7 GHz Effelsberg survey of the Galactic plane clearly demonstrating the anti-correlation between total intensities (upper panel) and polarized intensities (lower panel) [62, 70].

in Fig. 9, where the anti-correlation between total intensity and polarized intensity indicates depolarization by thermal matter, which is known to have a more narrow latitude distribution compared to synchrotron emission. The 2.7 GHz continuum and polarization survey data and also a number of other published radio survey data are freely available through the web from the MPIfR survey sampler: (<http://www.mpifr-bonn.mpg.de/survey.html>).

## 6.5 Running projects

The observations for the Effelsberg 1.4 GHz 'Medium Galactic Latitude Survey' (EMLS), which covers the Galactic plane from  $25^\circ$  to  $240^\circ$  in longitude for latitudes within  $20^\circ$ , is in an advanced stage of reduction [72]. Its observational methods and calibration procedures as well as a first set of example maps were published by Uyaniker et al. [73, 74]. The angular resolution of the EMLS is  $9''.4$ . It is confusion limited in total intensity at a rms-noise level of  $15 \text{ mK } T_b$ . The rms-noise in Stokes U and Q is about  $8 \text{ mK } T_b$ . Finally missing large-scale components will be added from the recently completed 26-m DRAO polarization northern sky survey, which is at an absolute temperature level [56]. Example maps from the EMLS are displayed in Figs. 11, 12 and 20.

The Effelsberg telescope was also used at 1.4 GHz to map a high latitude strip using a special observing strategy to recover also the large-scale polarization components. Preliminary results were published by Abidin et al. [75]. Higher structured

U and Q maps when compared to polarized intensity maps indicate the presence of substantial Faraday rotation at high latitudes even at 1.4 GHz. The fractional polarization level is up to about 30-40%.

The Arecibo 1000-ft telescope is planned to be used for a multi-beam L-band survey including linear polarization to be carried out by the GALFA Consortium [76]. The frequency from 1225 MHz to 1524 MHz will be covered simultaneously at about 3' angular resolution. A polarimeter with 1000 channels will be used. According to the sky accessible with the Arecibo telescope the observations will include sections of the Galactic plane, but also high latitude regions of the Galaxy.

Higher angular resolution polarization surveys at 1.4 GHz are underway from the DRAO synthesis radio telescope in the context of the 'International Galactic Plane Survey' (IGPS), previous CGPS ('Canadian Galactic Plane Survey')[68]. The IGPS (CGPS) project includes continuum, polarization, HI and CO observations at about 1' angular resolution and provides other complementary data as an unique basis for a wide range of Galactic studies. The 1.4 GHz polarization data are observed in four 7.5 MHz wide channels placed on either side of a central band, from which only HI images are derived. This allows the determination of RMs. An example polarization map is shown in Fig. 17. The Cygnus section from the polarization survey was published including an analysis of a variety of polarization structures by Uyaniker et al. [77]. Other polarization data from the CGPS were discussed elsewhere [e.g. 78-80].

The ATCA synthesis telescope was used to carry out the 'Southern Galactic Plane Survey' (SGPS) in continuum, linear polarization and HI at about the same angular resolution as the DRAO survey. The polarization data were collected in 12 bands, each 8 MHz wide, in the frequency range from 1332 MHz to 1436 MHz. A first section of the polarization survey was discussed by Gaensler et al. [81], up-dated information and more results from the SGPS are shown by Haverkorn et al. [82]. It is planned to complement the SGPS for missing large-scale components by additional observations with the Parkes 64-m telescope. Also the Villa Elisa southern sky polarization survey (Sect. 6.3) will be available to add the largest structures.

As already mentioned in Sect. 6.3 also new Westerbork polarization observations between 300 MHz and 400 MHz of large high Galactic latitude fields are in progress.

There are clear indications that polarization surveys available so far up to 1.4 GHz are mostly tracing emission structures of local origin. Comparing the all-sky total intensities (Fig. 1) and polarized intensities (Fig. 8) clear depolarization effects are indicated by the patchy and almost constant distribution of polarized emission for absolute latitudes below about 30° for the inner Galaxy. Depolarization of local origin is also obvious from Fig. 9 and Fig. 10. The distance ('polarization horizon' [78]) where entire depolarization along the line of sight occurs depends on the properties of the interstellar medium and also on the angular resolution of the observations. In general emission from much larger distances can be traced at high latitudes than close to the Galactic plane. Clearly observations at higher frequencies than 1.4 GHz or 2.7 GHz are needed. Currently the 25-m telescope at Nanshan station (Urumqi Observatory NAOC/China) is engaged in a 5 GHz polarization survey, which is a common NAOC/MPIfR project. At that frequency the distance range to observe polarized structures is about ten times larger than at 1.4 GHz. The intention of the

Urumqi observations are to map a similar area as covered by the 1.4 GHz EMLS survey. The angular resolution of  $9'5$  will be about the same for both surveys. To reach high sensitivities a re-build Effelsberg 5 GHz receiver and a broad-band polarimeter were installed at the Urumqi telescope. A brief description of the system was already given by Sun et al. [83]. The survey will be sensitive enough to trace polarized emission structures below 1 mK  $T_b$ . Recently also the Torun 30-m telescope is used for polarization observations of sections of the Galactic plane at 4.7 GHz using a MPIfR polarimeter [84].

The new 5 GHz polarization data need absolute calibration, which is not easy to perform at such high frequencies because of the weakness of the polarized signal in relation to systematic effects by the instrument and the environment. Efforts in this direction are undertaken at the Urumqi 25-m telescope. Alternatively some modelling of the high frequency signals based on absolute 1.4 GHz survey data [56] in combination with RM data from the Leiden-Dwingeloo surveys [45] might be used. These RM data, however, are derived from measurements between 408 MHz and 1.411 GHz, which is not ideal. Therefore it is planned to continue with polarization survey observations at the 26-m DRAO telescope in 2006 using a new multi-channel polarimeter to carry out the 'DRAO/MPIfR RM-Survey' for the northern sky above  $-30^\circ$  declination and about  $30'$  angular resolution with full sampling.

## 7 Analysis of polarized emission

### 7.1 Absolute calibration

The much more structured polarized emission when compared to the total intensity distribution calls for an explanation in terms of physical parameters of the magneto-ionic interstellar medium and numerous attempts have been already made so far. However, here must be a warning: all the new synthesis telescope surveys miss large-scale structures depending on the smallest baselines used. At very low frequencies the missing U and Q structures are likely small because of strong RM dispersion. Also surveys from large single-dish telescopes suffer from missing large-scale structures exceeding the size of the mapped region, although these scales are normally much larger than for synthesis telescopes. Structural interpretations of total intensities are rather little affected by these missing components, since a temperature offset or emission with a gradient across the feature of interest does usually not change its morphology. In polarization, however, the missing emission is a vector and when vectors are added the effect on the small-scale structures may be rather significant. For instance, enhanced small-scale emission may turn into a depression feature when adding large-scale emission or vice versa.

Several methods exist which combine low resolution with high resolution data. In case of the EMLS the combination with the Dwingeloo absolute polarization data was described by Uyaniker et al. [73]. In brief, the undersampled Dwingeloo U and Q data were interpolated to a regular grid and convolved. The corresponding Effelsberg data for the same field were convolved to the same effective beamwidth. Optionally spatial filtering may be applied to both maps. The difference to the Dwingeloo data was then interpreted as the missing large-scale component and is

## Latitude dependence of PI indicates a “local” origin

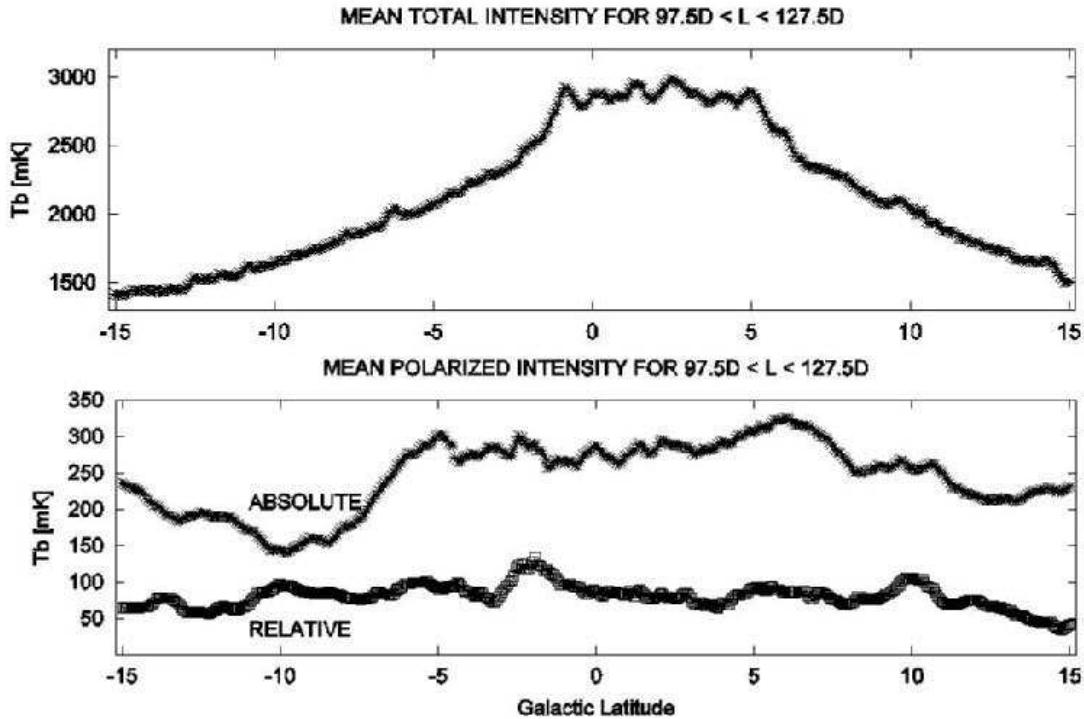


Figure 10: Averaged 1.4 GHz intensities from the EMLS for a section of the Galactic plane in the second quadrant shown as a function of Galactic latitude. Average polarized intensities are shown for the EMLS (‘Relative’) and after adding missing large-scale components from the Leiden-Dwingeloo survey (‘Absolute’, see Sect. 7.1).

finally added to the Effelsberg data at their original angular resolution of  $9'4$ .

Another technique is used when combining synthesis telescope data with single-dish data, where both maps are merged in the Fourier plane with appropriate weighting of the spatial frequencies in the range of overlap. In this case the smallest spacing of the synthesis telescope has to be smaller than the size of the single-dish telescope.

As already mentioned, the effect of adding the missing large emission in Stokes U and Q is non-linear for polarized intensity and the polarization angle (equations 3 and 4) and may result in significant changes in morphology. Also the distribution of polarized intensities and polarization angles changes. In Fig. 11 an example map from the EMLS is shown, where at the time of publication [74] no absolute polarization data were available. This field is located in the Galactic anti-centre a few degrees out of the Galactic plane, where the level of total intensity is quite low and dominated by extragalactic sources (see [74] for the total intensity image). Figure 12 shows the same field with large-scale U and Q components from the 26-m DRAO survey [43] added, which clearly causes morphological changes for most but not all small-scale features. The pixel spectrum of polarized intensities for both maps is shown in Fig. 13 for comparison, where the mean level of polarized emission differs by about 22 mK or about  $2\times$  the rms-noise of the original EMLS map.

In the case of high latitude fields the effect of missing large-scale structures causes

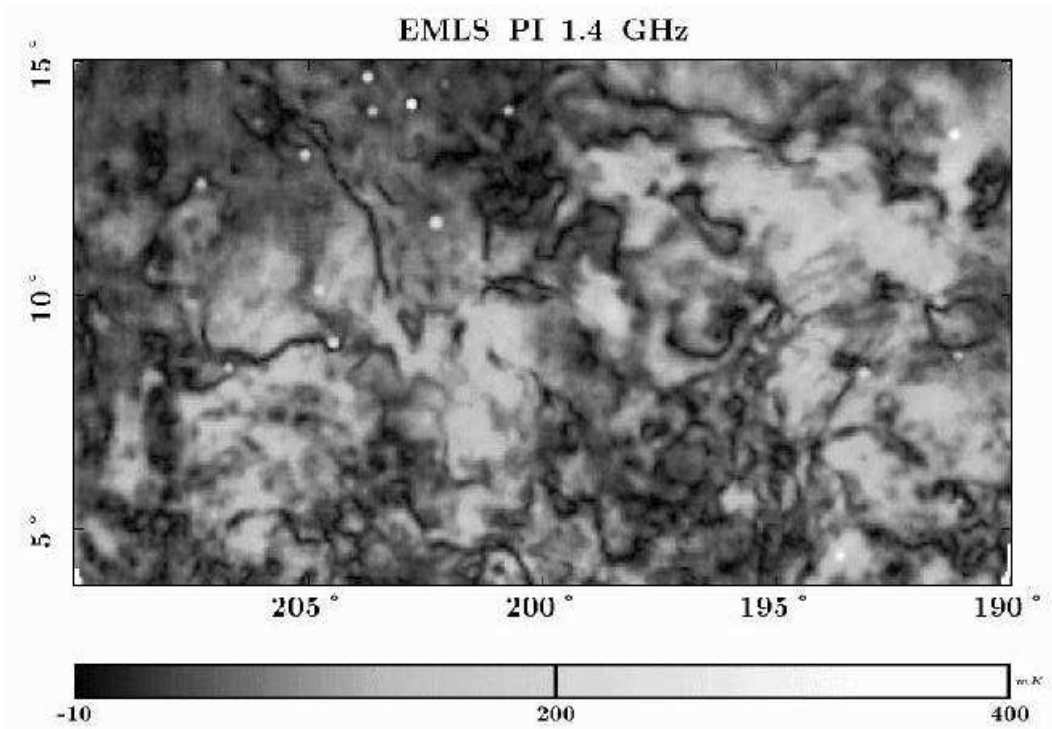


Figure 11: Map of 1.4 GHz polarized intensities as observed with the Effelsberg telescope [74] in a section of the Galactic anti-centre. The angular resolution is  $9''.4$  and the rms-noise in Stokes U and Q is 8 mK  $T_b$ .

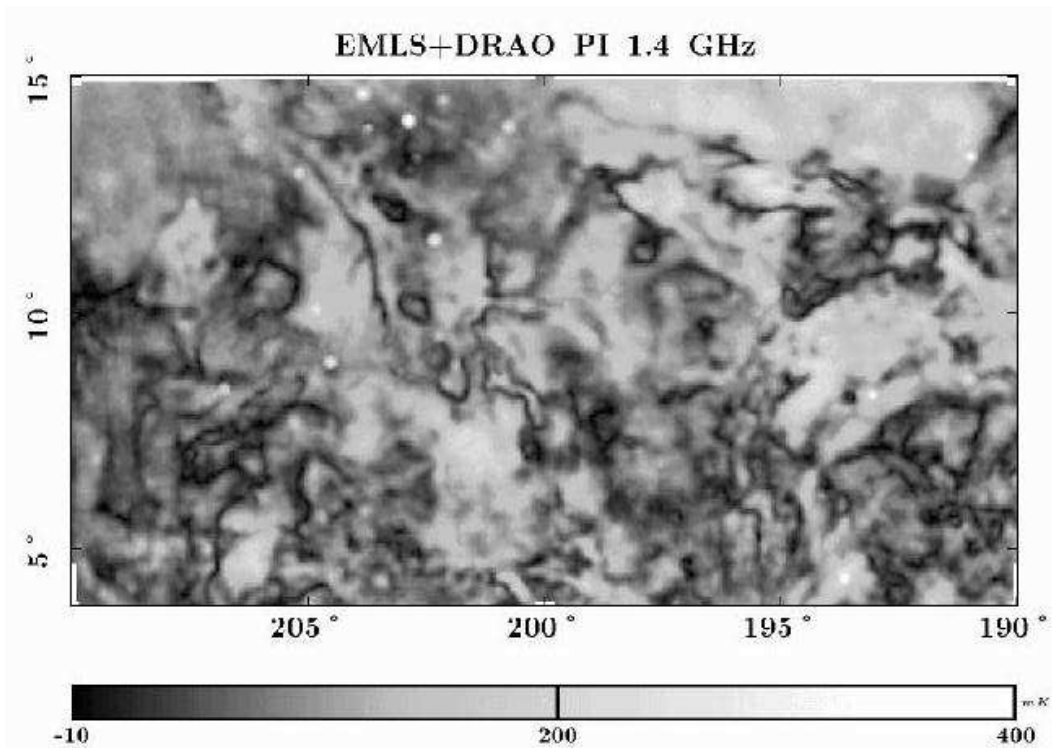


Figure 12: Polarization intensity map for the same field as in Fig. 11, but including large-scale data from the 26-m DRAO telescope [43].

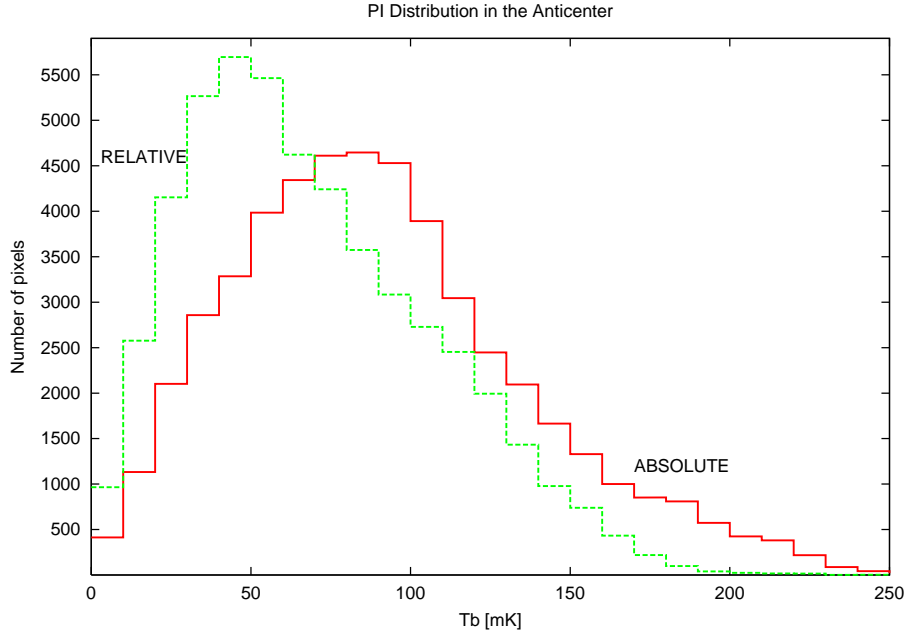


Figure 13: The polarized intensity spectrum for the Effelsberg map (Fig. 11) labeled 'Relative' and the Effelsberg map including large-scale components from the 26-m DRAO survey (Fig. 12) labeled 'Absolute'.

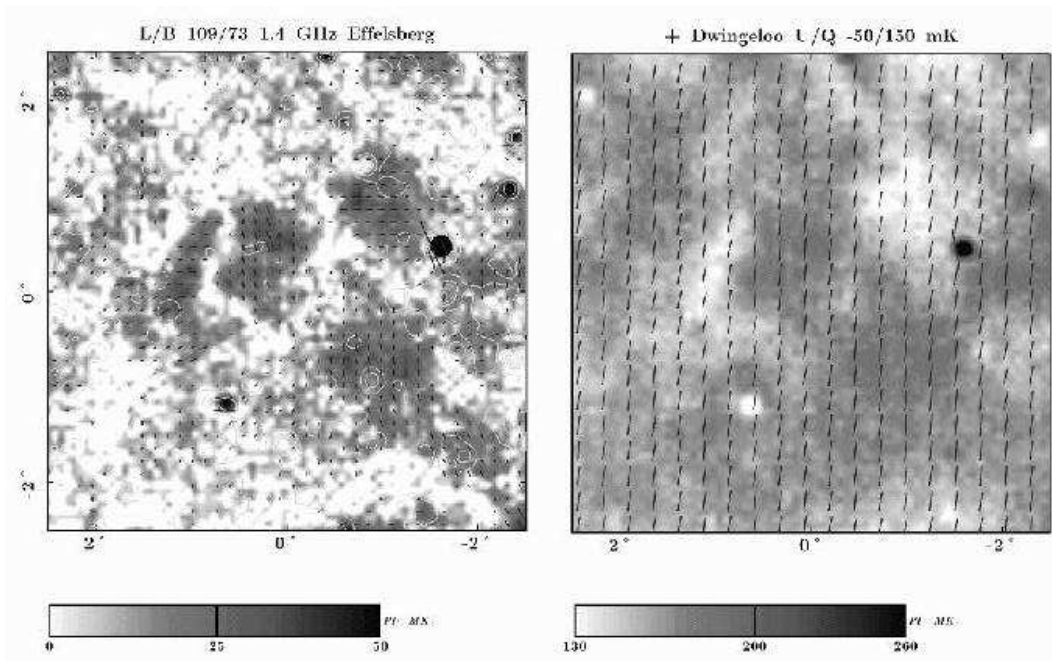


Figure 14: High latitude field centered at  $l, b = 109^\circ, 73^\circ$  observed with the Effelsberg 100-m telescope at 1.4 GHz (left panel). White contours indicate total intensities. The right panel shows the same map after addition of large-scale U and Q offsets taken from the Leiden-Dwingeloo survey [45]. Polarization bars are in E-field direction [85].

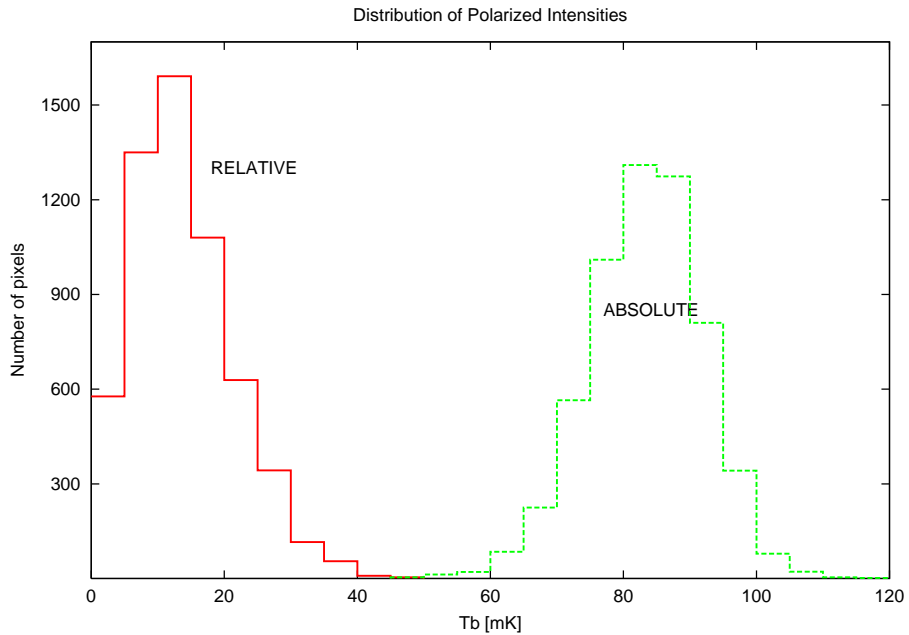


Figure 15: Pixel distribution of polarized intensities for the Effelsberg map (Fig. 14, left panel) labeled 'Relative' and the Effelsberg map including large-scale components from the Leiden-Dwingeloo survey [45] (Fig. 14, right panel) labeled 'Absolute'.

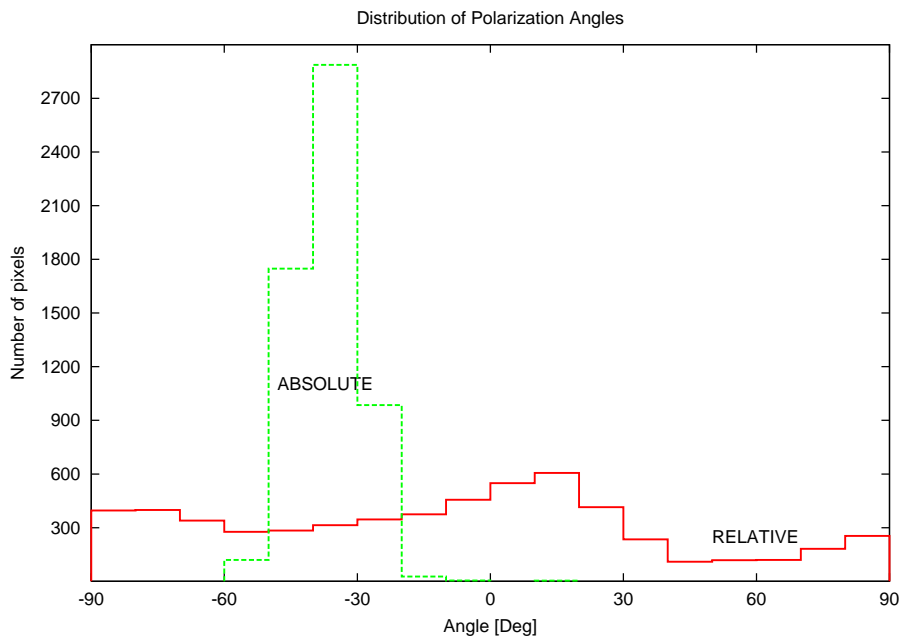


Figure 16: Pixel distribution as in Fig. 15, but for the polarization angles. Adding large offsets in U and Q largely reduces the range of polarization angle variations.

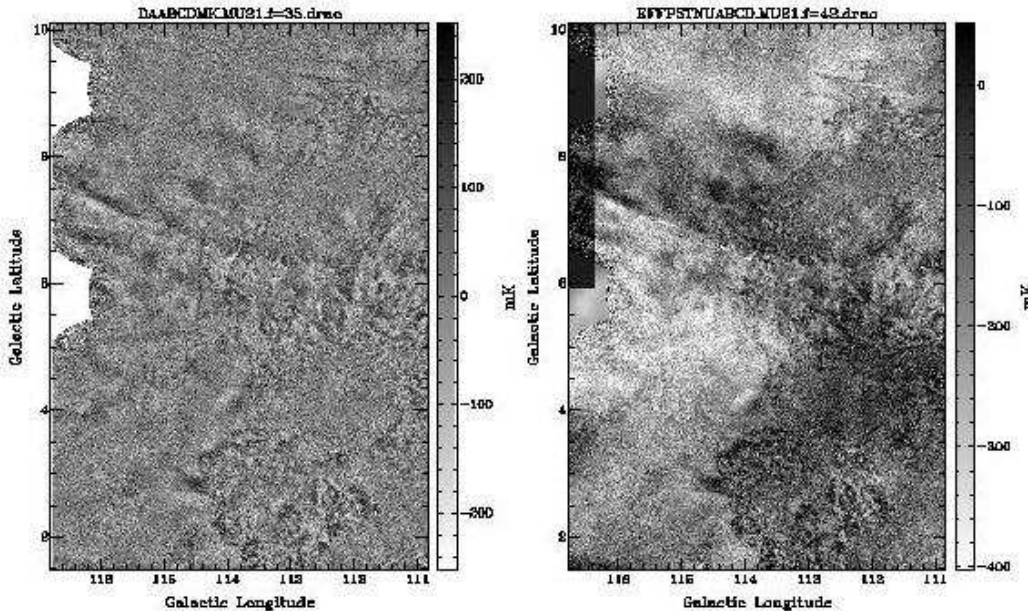


Figure 17: A Stokes U image using only DRAO interferometric CGPS data (left panel). A preliminary combination of Effelsberg 100-m and DRAO 26-m single-dish data with interferometric CGPS data (right panel). Note that what appeared to be a filament running North–South at  $l = 114^\circ$  in the lower half of the left panel is now revealed to be a front between two regions. The upper half of the right panel shows another front [86].

a dramatic change of the polarization morphology. Figure 14 (left panel) shows a  $5^\circ \times 5^\circ$  field observed at 1.4 GHz with the Effelsberg telescope in a similar way as the EMLS observations [85]. No extended total intensity features are seen exceeding a few times the noise level. However, numerous extragalactic sources dominate the field, a few of them are clearly polarized. The map of polarized intensities measured with the Effelsberg telescope shows a number of distinct patches with a typical size of about  $0.5^\circ$ . Typical peak polarized intensities are about 25 mK  $T_b$ . Figure 14 (right panel) shows the same field after adding the missing large-scale emission for this field. From the Leiden-Dwingeloo 1.411 GHz data [45] -50 mK in U and 100 mK in Q are estimated and added as constant offsets to the corresponding Effelsberg U and Q maps. The resulting differences in the polarized intensity maps and in the distribution of the polarization angles are large. After absolute calibration the polarized emission patches from the Effelsberg map are now seen either as enhancements of the uniform background polarization in case their polarization vectors are aligned with those of the diffuse large-scale emission. Otherwise they cause depressions in the polarized emission. Therefore the morphology of the polarized intensity distribution is totally different when the large-scale components are added. Because vectors are added also the structure function is changed. The distribution of the polarization angles is now reduced to small variations around a mean value for the field set by the dominant large-scale U and Q offsets. The strong changes are clearly reflected in the pixel distributions as displayed in Figs. 15 and 16.

From missing associated total intensity features in the Effelsberg map it is already

clear that the polarized patches must be caused by Faraday effects, which in view of the high Galactic latitude are likely not far distant from us. In general, local Faraday screens cause a larger observational effect on background polarization than more distant ones. There must be a difference in the magnetic field orientation of the foreground and the background emission that after Faraday rotation by a screen both fields are more aligned and thus the sum of both components exceeds the value seen outside of the screen. Also the opposite case occurs that by a screen's Faraday rotation the misalignment between foreground and background is enhanced. In that case a decrease of the polarized intensity is seen in respect to its surrounding. Multi-frequency data to calculate RMs are needed to decide whether the differences in Faraday rotation are due to fluctuations around a certain (large enough) RM value or the magnetic fields in the Faraday screens have an opposite direction.

An example for the differences in morphology and physical interpretation resulting from combining EMLS single-dish map with higher resolution CGPS data from the DRAO synthesis telescope is shown in Fig.17. Some filamentary structures seen as isolated features in the CGPS map are revealed to mark the boundary between different extended regions when the single-dish data are included [86].

## 7.2 RM determination

The RM of the diffuse Galactic emission was determined by various authors using available low frequency polarization surveys [42, 45]. Figure 18 shows an example for a RM-map calculated by Spoelstra [46]. RMs were determined by fitting a linear slope to the observed polarization angles as a function of  $\lambda^2$ . RM maps from low frequency surveys show all quite low values, in particular when compared to the RM values from extragalactic sources in the field, which trace the Faraday rotation from the entire interstellar medium along the line of sight through the Galaxy and do almost not suffer from depolarization effects. The conclusion from this result is that the observed diffuse low frequency polarized emission is of local origin. Of course, the early RM maps should be interpreted with some care. A valid RM determination requires that the emission originates from the same volume, which is questionable when data at 408 MHz are compared with those at 1.4 GHz, except when they are very local. In addition, the observation should have the same beamwidth to avoid an effect from polarization vector averaging across the area of the beam, except that the emission region has a very uniform distribution of polarization vectors and is larger than all the beams involved.

Today's RM determination from multi-channel narrow-band polarimeter avoid these effects. Gaensler et al. [81] using the ATNF compact array (ATCA) in connection with a multi-channel backend for mapping the polarized emission of the southern Galactic plane obtain rather high RM values ranging within about  $\pm 150 \text{ rad m}^{-2}$  in the direction of thermal emission regions. However, the ATCA data miss the large-scale emission components and these may well influence the RM values measured and thus their physical interpretation. A new project to determine the RM distribution of the diffuse polarized Galactic emission on an absolute scale at L-band, where the beamwidth variations over the band are small, will start soon at the 26-m DRAO telescope (see Sect. 6.5).

The  $\lambda^2$  dependence of polarization angles is an important diagnostic tool [see

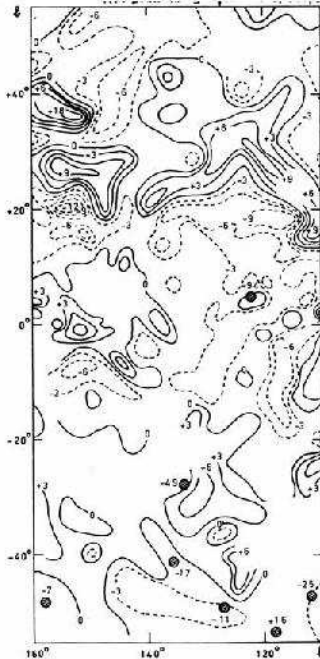


Figure 18: RM map based on the Leiden-Dwingeloo polarization surveys covering partly the Cetus Arc and Loop III [46]. The black dots indicate RM values for extragalactic sources, which are in general much larger than the RM values for the diffuse Galactic emission as observed at low frequencies.

38], however, it is destroyed in case of the superposition of various polarization components with different RM or by depolarization effects or by missing large-scale structures. From two frequency observations one can not decide whether the  $\lambda^2$  dependence is given and thus RMs should be taken with care. The correct interpretation of observed RMs needs additional modelling efforts, for instance, to determine the physical parameter of passive Faraday rotating structures ('Faraday Screens') at a certain distance (see Sect. 7.4).

### 7.3 Depolarization effects

Faraday rotation in the interstellar medium along the line of sight leads to depolarization. In addition there are instrumental effects as the beamwidth and the bandwidth of the observation, which also might cause depolarization. All these effects have been already extensively discussed in the literature and are briefly summarized here:

*Bandwidth depolarization* occurs when the polarization angles vary across the frequency band, which reduces the observed amount of polarized emission. The depolarization DP, which is defined as  $DP = PC_{obs}/PC_{int}$ , the ratio between the observed and the intrinsic polarization, calculates as  $DP = \text{sinc}(2 \text{ RM } \lambda^2 \delta\nu/\nu)$ , where  $\delta\nu$  is the bandwidth of the observations. For narrow observing bands, high frequencies or small RM values DP becomes negligible.

*Beam depolarization* occurs in case polarization vectors of different orientation are unresolved by the telescope beam. In order to separate *beam depolarization*

from depolarization effects in the interstellar medium polarization data measured at different wavelengths must be compared at the same angular resolution.

In his classical paper Burn [40] discussed differential Faraday rotation (was also called depth depolarization), internal Faraday dispersion and Faraday dispersion in an external screen. These basic concepts and formula are most often used in the interpretation of polarized emission. Of course, it is rather obvious that more complex scenarios than the uniform distribution of the magneto-ionic components are required to describe recent Galactic polarization observations [38]. Sokoloff et al. [87] made an attempt in that direction and demonstrate that non-uniform effects have a strong effect on the observed polarization distribution.

Burn's 'slab model' [40] is often used to calculate the *internal depolarization* of a source, where thermal electrons, relativistic electrons and magnetic fields are uniformly mixed. Then DP calculates as  $DP = \text{sinc}(2 RM \lambda^2)$ . For the case of significant RM fluctuations  $\sigma_{RM}$  one gets  $DP = \left| \frac{1 - \exp(-S)}{S} \right|$ , where  $S = 2 \sigma_{RM}^2 \lambda^4 - 4i \lambda^2 RM$ . *External depolarization* depends entirely on  $\sigma_{RM}$  in the foreground medium:  $DP = \exp(-2\sigma_{RM}^2 \lambda^4)$  (for more details see [87]).

## 7.4 Faraday screens

Excessive Faraday rotation in the magneto-ionic interstellar medium may be caused either by an enhanced thermal electron density or by a stronger or more regular magnetic field component along the line of sight. For example, RM values of extragalactic sources may be enhanced when observed in the direction of a HII-region. Strong magnetic fields are known to exist in the shells of SNRs as the result of interstellar magnetic field compression by their expanding shock fronts, which cause a strong increase of the synchrotron emissivity and in most cases also strong linear polarization. In addition to Faraday rotating sources with a clear signature in total intensities, the polarization surveys reveal a class of Faraday screens, which are very weak or invisible (at a certain sensitivity level) in the corresponding total intensity survey map, but impose clear effects in the polarization angle distribution and/or the polarization intensity distribution. In some cases weak  $H_\alpha$  emission can be seen, but for many Faraday screens available  $H_\alpha$  surveys seem not to be sensitive enough to trace them and just allow to derive an upper limit for the thermal electron density. These Faraday screens have a low electron density and thus need an enhanced regular magnetic field along the line of sight direction to account for the observed Faraday rotation. Discrete Faraday screens were first reported and discussed by Gray et al. [88] and Wieringa et al. [47].

Any interpretation of the observed RMs towards a Faraday screen needs its distance to get its physical parameters. This is in general not easy to measure. Wolleben and Reich [89, 90] made observations of Faraday screens located nearly exactly at the boundaries of some Taurus molecular clouds, for which the distance is known to be 140 pc. A full analysis of absolutely calibrated data, which are at least needed at two frequencies, gives information on the physical properties of the Faraday screens and the fraction of foreground to background polarized emission for its distance. The observations used in this study are from the Effelsberg 100-m telescope at 1408 MHz, 1660 MHz and 1713 MHz. Zero-spacings were added from the 1411 MHz Leiden-Dwingeloo survey to the 1408 MHz map. Zero-spacings for the

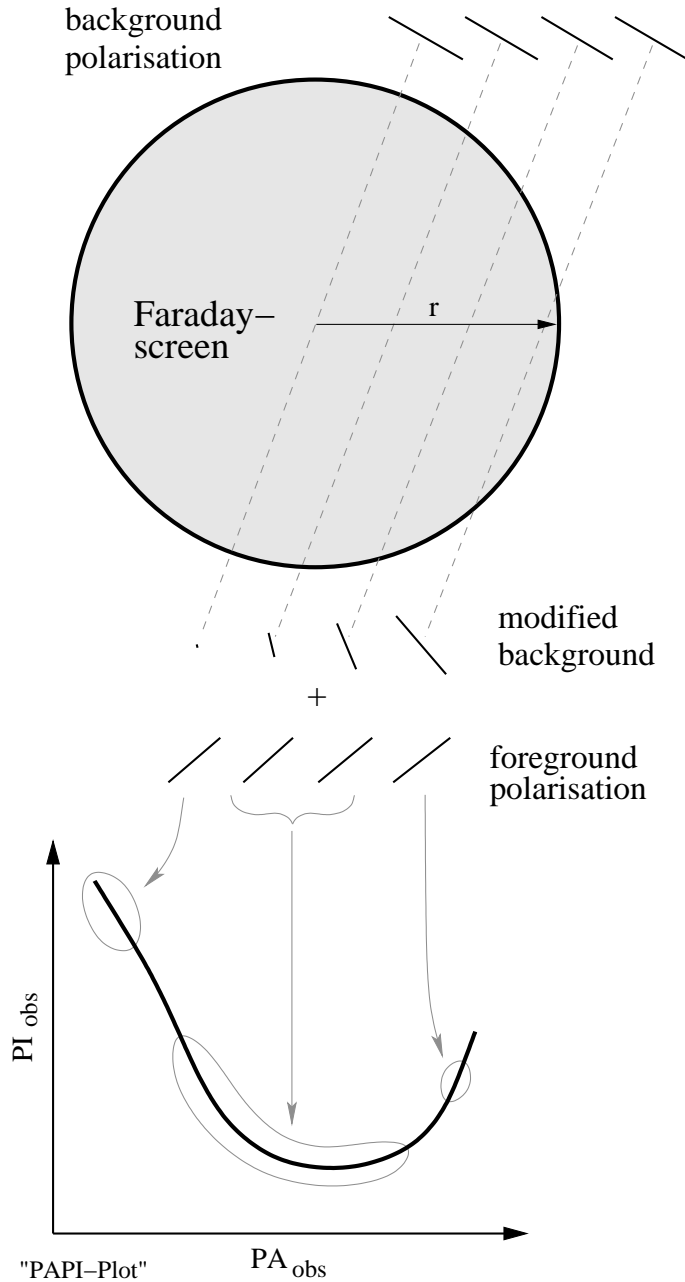


Figure 19: A spherical cloud acting as a Faraday screen. The line of sight length through the cloud is taken as proportional to RM (and also to DP). The background polarization is modified by the Faraday screen and adds to the foreground polarization. The observed polarization for such a region has a characteristic polarization intensity versus polarization angle dependence (PAPI-plot). Based on this model multi-frequency polarization data at an absolute level were analysed by Wolleben and Reich [89, 90] to derive physical parameters of Faraday screens located at the boundaries of local molecular clouds in the Taurus region. Also the properties of the Galactic foreground and background polarization can be determined by the model.

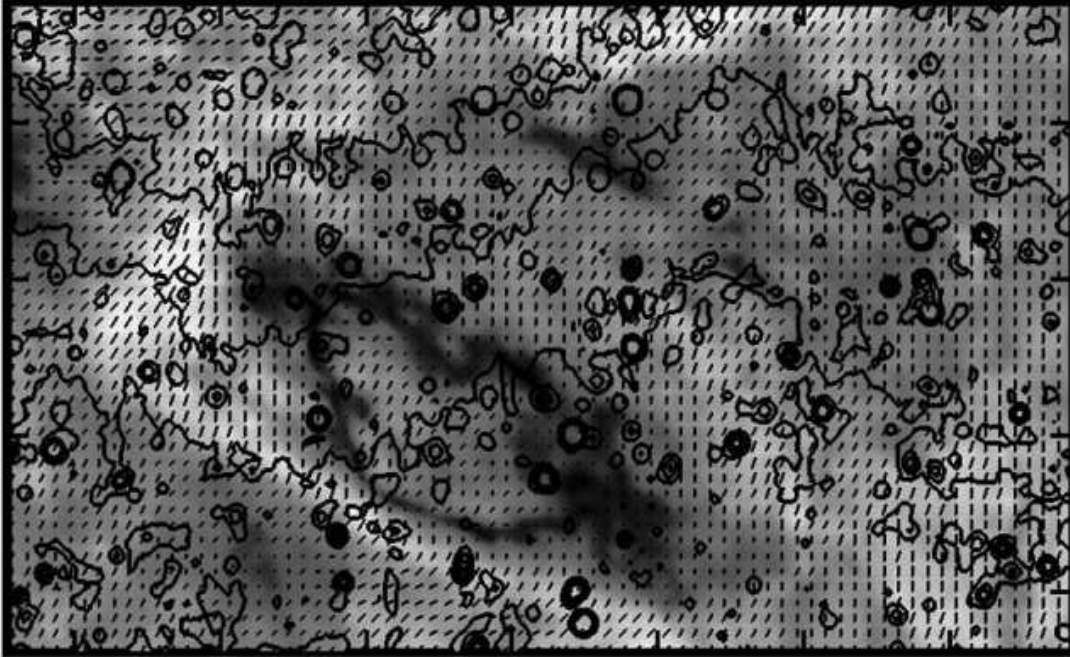


Figure 20: Section of the 1.4 GHz EMLS (mapcentre at  $l = 114^{\circ}1, b = -10^{\circ}6$ , mapsize  $14^{\circ}6 \times 8^{\circ}3$ ) with large-scale emission added from the Dwingeloo survey [45]. The map of polarized intensities (greyscale coded) shows an elliptical shell like feature with up to  $8^{\circ}$  in size. Polarization E-vectors are superimposed. There is no counterpart in total intensities (shown by contours) indicating systematic Faraday rotation by a shell structure of unknown distance.

other two frequencies were extrapolated with a spectral index of  $\beta = -2.7$ , which is close to the total intensity spectral index. It was also assumed that  $RM = 0 \text{ rad m}^{-2}$  is valid for the diffuse emission in this area (see Fig. 18,[46]). These assumptions seem quite reasonable, but also reflect the fact that the availability of absolutely calibrated data and RM information is rather limited.

Nine Faraday screens were analysed, where the observed RM varies between  $-36 \text{ rad m}^{-2}$  and  $+26 \text{ rad m}^{-2}$ . The typical size of the individual objects is about 2 pc. The Faraday screens selected are seen as minima in the polarized intensity map at 1408 MHz. At the two higher frequencies the minima are less pronounced or already disappeared. Thus the spectral indices calculated for the minima ranges from  $\beta = -1.3$  to  $+2.0$ . The Faraday screen data were then analysed in terms of the model shown in Fig. 19, where a spherical cloud imposes Faraday rotation and in addition depolarization (DP) on the background polarized emission, which then adds to the foreground emission as observed. As a result of the model the foreground and the background polarization is obtained and additionally the RM and the DP of the Faraday screen. For the Taurus clouds always negative RMs were derived ranging between  $-18 \text{ rad m}^{-2}$  and  $-29.5 \text{ rad m}^{-2}$ . This result clearly demonstrates that the RM for Faraday screens in general is rather different to the directly observed RM. The foreground polarization angles scatter around  $0^{\circ}$ , while the background polarization angles vary within  $-10^{\circ}$  and  $-19^{\circ}$ .

In the case of the Taurus clouds additional information of the emissivity of the synchrotron emission can be obtained by using the maximal fractional limit imposed

by the polarized emission to calculate the minimum total synchrotron emission. For the local Taurus clouds enhanced synchrotron emission in this direction results, which is in agreement with other estimates [89].

Another elliptically shaped Faraday screen from the EMLS is shown in Fig. 20, which imposes more complex although systematic effects on its background emission. The polarized emission seen towards its centre seems basically undisturbed (compared to the surroundings of the Faraday screen), for larger radii first a minimum is seen, followed by a maximum in polarized emission. This clearly indicates systematic variations of the Faraday rotation by some shell like structure, so that the rotated background emission enhances or reduces the observed polarization when added with the foreground. So far no distance information is available for this Faraday screen, which is required to estimate its physical parameters.

A huge magneto-ionic bubble acting as a Faraday Screen was recently reported by Kothés et al. [91] using for the first time combined polarization data from the DRAO 26-m telescope, the Effelsberg 100-m telescope and the DRAO synthesis telescope. The preliminary analysis of this shell in the Galactic anti-centre gives a diameter of about 400 pc at a distance of 2 kpc. A HI-shell coincides with the bubble and locates it in the Perseus arm. The origin of the bubble is likely from a stellar wind. The object can be modelled by the following parameters: shell thickness 40%, electron density  $0.07 \text{ cm}^{-3}$  and a magnetic field strength of  $16 \mu\text{G}$ .

The problem when analysing Faraday screens from data not at an absolutely calibrated level may be illustrated by the case of G91.8-2.5. Data from the DRAO synthesis telescope give a  $\delta\text{RM}$  of about  $40 \text{ rad m}^{-2}$  measured around 1.4 GHz [92], while RMs from Effelsberg multi-channel observations in the same frequency range give  $\text{RM} = -27 \text{ rad m}^{-2}$  [93]. This makes a polarization angle difference of more than  $30^\circ$  and reflects a different amount of large-scale structures missing in the synthesis telescope data and the single-dish map. In both cases it seems problematic to use the measured RM values to derive physical parameters for the Faraday screen. Its distance is needed and some modelling is required.

Low frequency polarization spectra were modelled by Vinyajkin [94] for selected regions of the Galaxy based on an assumed multi-layer structure of the magnetized interstellar medium. Vinyajkin's model is able to describe the observed absorption dips at specific frequencies, which are superimposed on the power law spectrum of the polarized emission and complements effects caused by Faraday screens. At low frequencies small RM variations already cause large changes on the polarized structures, while at higher frequencies larger RMs as revealed by discrete Faraday screens are needed for observable polarization effects.

Figure 21 shows an example of the influence of a discrete Faraday screen on the observed polarized intensities. In this case the RM of the interstellar medium is assumed to have  $\text{RM} = 0 \text{ rad m}^{-2}$  along the entire line of sight and thus the Faraday screen always causes a depression, whose amount depends on its location within the diffuse interstellar medium. The minimum polarized intensity is observed for equal foreground and background emission. It is easily seen from Fig. 21 that Faraday screens of different RM located at different distances in the interstellar medium are able to create a rather complex distribution of polarized intensities even though the diffuse magneto-ionic interstellar medium has very uniform properties. It is also evident that at higher frequencies the Faraday screens need to have large RMs to

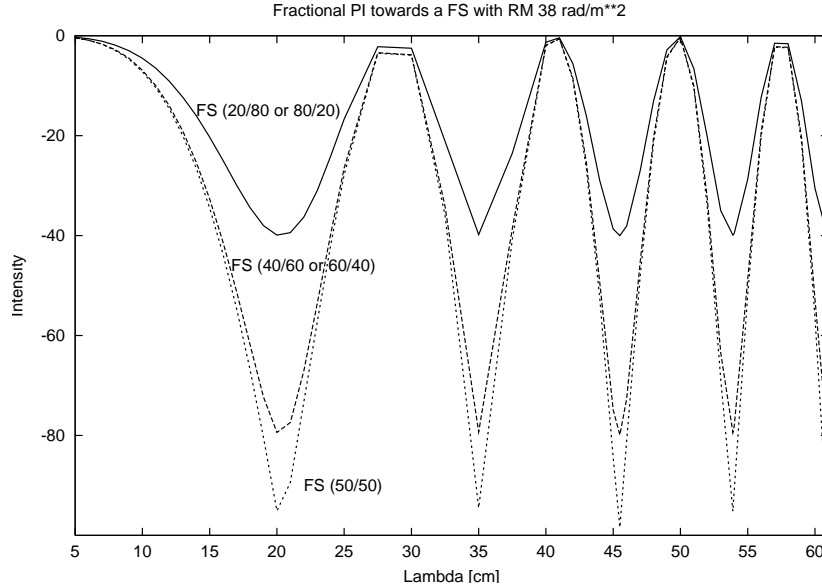


Figure 21: Fractional polarization (relative to its surroundings) seen towards a Faraday screen with a RM of  $38 \text{ rad m}^{-2}$  as a function of wavelength. The interstellar medium along the line of sight is assumed to be homogenous with  $\text{RM} = 0 \text{ rad m}^{-2}$ . The fractional polarization is calculated for different ratios for the foreground to background emission. In this quite simple case absolute intensity minima are expected when foreground and background emission relative to the Faraday screen are the same.

cause an effect on the polarized distribution. High frequency polarization observations are needed to reveal the intrinsic properties of the magnetic field distribution in the interstellar medium.

Optically thin HII-regions may act as Faraday screens by depolarizing their background polarization. They become optically thick at low frequencies, depending on their electron density and temperature. Because their distance can be independently determined, they are ideal objects for 'Galactic tomography'. At low frequency the foreground total intensity can be measured as they fully absorb the background emission. At sufficiently high frequencies (depending on their distance) the corresponding foreground polarization component is observed. Thus future high angular resolution low frequency observations, as they will become possible with the LOFAR telescope, when combined with high frequency polarization observations, e.g. from the Effelsberg 100-m telescope, will provide detailed information on the magnetic field components within a few kpc and the distribution of the thermal gas components [95]. Low frequency absorption spectra need some modelling of the components of the thermal gas along the line of sight [96]. These results will constrain Faraday screen models describing the radiation transfer of polarized emission.

## 7.5 Canals

Maybe the most striking unusual structures in the various new polarization survey maps with sufficiently high angular resolution are long narrow nearly depolarized features commonly named 'canals'. They are for example clearly visible in Fig. 11

or Fig. 12. Most of these 'canals' have similar properties: their width is about one beam and the polarization angles change from one side of the 'canal' to the other by  $90^\circ$ . This requires a gradient for the U and Q intensities perpendicular to the 'canals'. At the 'canal' itself U and Q become zero.

So far two explanations have been published on the origin of the 'canals': beam depolarization [54, 55] caused by a sufficiently large RM gradient within one beam and Faraday depth depolarization [97] in a uniform synchrotron emitting magneto-ionic medium. In the case of beam depolarization the 'canals' do not change their position with frequency, but at high frequencies 'canals' require very large RM changes across a beam. At 350 MHz a RM gradient across a beam of about  $2.1 \text{ rad m}^{-2}$  is sufficient and no unusual properties of the interstellar medium are needed. Some numerical models of a Faraday rotating interstellar medium supports this interpretation of low frequency observations [55]. At 4.8 GHz, however, the RM gradient across a beam width must be  $400 \text{ rad m}^{-2}$  to cause a 'canal', which seems to be an unrealistic high value for the interstellar medium in general and therefore 'canals' observed at high frequencies most likely need another explanation. Shukurov and Berkhuijsen [97] propose differential Faraday rotation as an explanation for the 'canals': The 'canals' represent 'level lines' of RM. Because they are no physical structures they have been called 'Faraday ghosts'. The separation of the 'canals', however, provides useful information on the turbulent interstellar medium.

It must be noted that the discussion of 'canals' above is in all cases based on relative (synthesis telescope) rather than absolute polarization data. Shukurov and Berkhuijsen [97] comment on various aspects of that problem. Obviously some conclusions reached for the 'canals' might change when the large-scale polarized emission is available and has been properly taken into account.

## 7.6 RM data from pulsars and extragalactic sources

RM data from pulsars and extragalactic sources are potentially very valuable for the interpretation of diffuse Galactic polarized emission as they trace the entire line of sight component of the Galactic magnetic field in a certain direction. They are thus complementary to the perpendicular component of the magnetic field as seen from synchrotron emission. However, tomography is needed to reveal information on the magnetic field and the thermal electron density along the line of sight. Figure 18 illustrates the relation of RMs of extragalactic sources in a certain area to the RMs measured for the diffuse polarized Galactic emission.

In particular RM data from pulsars are useful to analyse the Galactic magnetic field as they provide in principle in combination with the measurable dispersion measure (DM) the line of sight magnetic field strength (however see [98] for related problems). While the RM of a single pulsar is helpful, for instance, to estimate the foreground effect of the interstellar medium towards polarized SNRs, fairly large RM samples are needed for a reliable estimate of the local structure, direction and intensity of the magnetic field. Current estimates give a regular magnetic field strength around  $1.4 \mu\text{G}$  in the direction of the local arm with a pitch angle of a few degrees [27, 28, 29, 30], which is small when compared to the total magnetic field strength (see Sect. 4.2). Also magnetic field reversals between different spiral arms of the Galaxy are based on pulsar RM as discussed in Sect. 4.2.

There are various observation projects actually carried out aiming to increase the number of pulsar RMs and the RMs of extragalactic sources. In particular from synthesis telescope surveys, where narrow band polarimetry is available, a large number of RMs of sources located in the Galactic plane were measured in the course of the Canadian Galactic Plane Survey (CGPS) [68] and the Southern Galactic Plane Survey (SGPS) [81] (see Sect. 6.5). These densely sampled RM data of extragalactic sources are obtained at 1.4 GHz with a beam of about  $1'$  [82, 99]. At higher latitudes single-dish telescopes are used to increase the number of RMs of extragalactic sources. A project was recently completed to measure 1800 polarized NVSS sources with the Effelsberg 100-m telescope mostly located out of the Galactic plane using multi-channel polarimetry at 21cm/18cm [Han et al., in prep.].

The potential of a very dense grid of RM data from pulsars and extragalactic sources for a detailed analysis of the properties of the Galactic magnetic field on all relevant scales and also for the evolution of magnetic fields in galaxies is widely accepted. Consequently one of the key-projects for the planned Square Kilometer Array (SKA) is a RM survey providing RM data for some tens of million sources [100]. This RM survey is planned as part of a global sky survey in the 1.4 GHz range. Based on model predictions about 2900 polarized sources per  $\text{deg}^2$  stronger than  $1 \mu\text{Jy}$  are expected and about 50% of them should have a measurable RM. This gives about  $2 \cdot 10^7$  RMs from the survey with a mean distance of about  $90''$  between the sources. This holds for a 1 h integration time with the SKA. An increase of the integration time to 10 h will reduce the mean RM spacing in that field to  $40''$  [100]. Details on numerous important scientific applications of such a dense RM grid were discussed by Beck and Gaensler [100].

## 8 Status and Outlook

The revival of Galactic polarization surveys over the last years has led to intensive discussions on the composition and structure of the Galactic magneto-ionic medium. Numerous workshops and conferences were held during the last years and the proceedings reflect the observational status as well as the progress achieved in modelling the magneto-ionic interstellar medium [101-104].

Many large polarization surveys are in progress today mostly around 1.4 GHz. The direction of future observations is towards higher frequencies, where local Faraday rotation effects are less important and the Galaxy becomes transparent even in the disk. Such measurements require high sensitivity equipment because of the weakness of the polarized signals. Multi-channel polarization observations in numerous narrow bands are another observational direction, which in combination with advanced analysis methods [38] is quite powerful to decompose complex superimposing polarization structures along the line of sight. The analysis of the planned L-band RM-survey with the DRAO 26-m antenna (see Sect. 6.5) relies on this technique.

Absolutely calibrated polarization data at high frequencies (above 1.4 GHz) for large-scale emission is another indispensable need for the proper analysis of polarization data. Unfortunately such data are not easy to obtain at high frequencies. Beside sensitive receivers also a very high stability of the entire receiving system is

needed as well as a low level of the telescope’s far-sidelobes. Such measurements are time consuming, but can be done with small telescopes. However, they must be located at well selected suitable sites.

Galactic polarization is considered as an important foreground for future sensitive Cosmic Microwave Background (CMB) polarization observations. Polarization surveys available in numerical form as the Leiden-Dwingeloo large-scale survey were analysed in terms of their angular power spectrum by various authors [105 and references therein]. Also the new large-scale polarization surveys are actually analysed in a similar way [106]. Of course, also for the various recent Galactic plane surveys with higher angular resolution the angular power spectrum is available although they are more influenced by Faraday effects than high latitude regions [107 and references therein]. A problem with available Galactic polarization data are their low frequencies and the influence of Faraday effects when compared to the much higher frequencies, where CMB observations are carried out. Source contamination of the angular power spectrum turns out to be severe, depolarization effects vary with frequency and only at high Galactic latitudes one can be sure to look out off the Galaxy. Thus extrapolations towards higher frequencies are not easy to perform with high accuracy, but upper limits can be given with confidence.

High frequency observations above 1.4 GHz are needed. 2.7 GHz and 5 GHz observations are already on the way, which may better constrain foreground predictions at CMB frequencies in general than it is possible with available data. However, recent results for selected fields with low synchrotron and dust emission are promising. CMB Polarization (CMBP) is usually expressed in terms of E- and B-modes [e.g. 108], where the E-mode is at a few percent of the CMB anisotropies, but the level of the much weaker B-mode is largely unknown. However, the B-mode is needed to disentangle different Inflation models [109]. Sensitive observations of a northern and southern target selected for CMB Polarization (CMBP) observations [110] by the BaR-SPOrt experiment [111] were recently carried out. 1.4 GHz observations with the Effelsberg 100-m telescope of the northern BaR-SPOrt field, which is at very high Galactic latitude, reveals the lowest contamination by polarized Galactic foreground emission measured so far. This implies good chances to detect B-mode emission at about 90 GHz [112]. More extended searches may reveal areas with are suited to detect even weaker B-mode signals. Therefore the polarized Galactic synchrotron foreground seems not to be a limitation to detect weak CMBP signals at least on scales up to a few degrees in extent.

## 9 Acknowledgement

I like to thank Ernst Fürst and Patricia Reich for sharing common efforts over many years on Galactic survey projects and their critical comments on the manuscript. I acknowledge discussions and cooperation with Roy Duncan, JinLin Han, Roland Kothes, Tom Landecker and Rob Reid on polarization survey issues. I am grateful to Richard Wielebinski for initiating and strongly supporting the various MPIfR survey projects over the last 30 years. Without his engagement the new 5 GHz polarization surveys would not been possible. Former PhD-students made significant contributions to the different survey projects at the MPIfR in Bonn: Norbert Junkes,

Juan Carlos Testori, Buelent Uyaniker and Maik Wolleben. Helpful discussions with Rainer Beck on the manuscript are acknowledged too.

## 10 References

1. C.H. Mayer, T.P. McCullough, and R.M. Sloanaker, 1957, *Astrophys. J.*, 126, 468
2. G. Westerhout, C.L. Seeger, W.N. Brouw, and J. Tinbergen, 1962, *Bull. Astron. Inst. Netherlands*, 16, 187
3. R. Wielebinski, J.R. Shakeshaft, and I.I.K. Pauliny-Toth, 1962, *The Observatory*, 82, 158
4. R. Wielebinski, and J.R. Shakeshaft, 1964, *MNRAS*, 128, 19
5. E.M. Berkhuijsen, and W.N. Brouw, 1963, *Bull. Astron. Inst. Netherlands*, 17, 185
6. D.S. Mathewson, N.W. Broten, and D.J. Cole, 1965, *Austr. Journal of Physics*, 18, 665
7. C.A. Muller, E.M. Berkhuijsen, W.N. Brouw, and J. Tinbergen, 1963, *Nature*, 200, 155
8. E.M. Berkhuijsen, W.N. Brouw, C.A. Muller, and J. Tinbergen, 1964, *Bull. Astron. Inst. Netherlands*, 17, 465
9. R.G. Bingham, 1966, *MNRAS*, 134, 327
10. D.S. Mathewson, N.W. Broten, and D.J. Cole, 1966, *Austr. Journal of Physics*, 19, 93
11. E.M. Berkhuijsen, 1975, *Astron. Astrophys.*, 40, 311
12. A.G. Pacholczyk, 1970, *Radio Astrophysics*, San Francisco, W.H. Freeman
13. P. Reich, 2003, *Acta Astronomica Sinica*, Vol. 44 Suppl., 130
14. J.L. Jonas, E.E. Baart, and G.D. Nicolson, 1998, *MNRAS*, 297, 977
15. C.L. Bennett, M. Halpern, G. Hinshaw, et al., 2003, *ApJS*, 148, 1
16. R. Wielebinski, 2005, in 'Cosmic Magnetic Fields', Eds. R. Wielebinski, R. Beck, *Lect. Notes Phys.* 664, Springer, 89
17. W. Reich, 1982, *Astron. Astrophys. Suppl.*, 48, 219
18. P. Reich, and W. Reich, 1986, *Astron. Astrophys. Suppl.*, 63, 205
19. P. Reich, J.C. Testori, and W. Reich, 2001, *Astron. Astrophys.*, 376, 861

20. P. Reich, W. Reich, and J.C. Testori, 2004, in 'The Magnetized Interstellar Medium', Eds. B. Uyaniker, W. Reich, R. Wielebinski, Copernicus GmbH, 63
21. R. Beck, 2005, in 'Cosmic Magnetic Fields', Eds. R. Wielebinski, R. Beck, Lect. Notes Phys. 664, Springer, 41
22. M. Krause, 2004, in 'The Magnetized Interstellar Medium', Eds. B. Uyaniker, W. Reich, R. Wielebinski, Copernicus GmbH, 173
23. K. Beuermann, G. Kanbach, and E.M. Berkhuijsen, 1985, *Astron. Astrophys.*, 153, 17
24. S. Phillipps, S. Kearsy, J.L. Osborne, C.G.T. Haslam, and H. Stoffel, 1981, *Astron. Astrophys.*, 98, 286
25. C.G.T. Haslam, H. Stoffel, C.J. Salter, and W.E. Wilson, 1982, *Astron. Astrophys. Suppl.*, 47, 1
26. A.W. Strong, I.V. Moskalenko, and O. Reimer, 2000, *ApJ*, 537, 763
27. R.J. Rand, and A.G. Lyne, 1994, *MNRAS*, 268, 497
28. J.L. Han, and G.J. Qiao, 1994, *Astron. Astrophys.*, 288, 759
29. C. Indrani, and A.A. Deshpande, 1999, *New Astronomy*, 4, 33
30. J.L. Han, R.N. Manchester, A.G. Lyne, and G.J. Qiao, 2002, *ApJ*, 570, L17
31. A. Shukurov, 2005, in 'Cosmic Magnetic Fields', Eds. R. Wielebinski, R. Beck, Lect. Notes Phys. 664, Springer, 113
32. J.H. Taylor, and J.M. Cordes, 1993, *ApJ*, 411, 674
33. J.M. Cordes, and T.J.W. Lazio, 2005, *astro-ph\0207156*
34. C.K. Lacey, T.J.W. Lazio, N.E. Kassim, N. Duric, D.S. Briggs, and K.K. Dyer, 2001, *ApJ* 559, 954
35. K.R. Anantharamaiah, 1986, *J. Astrophys. Astron.*, 7, 131
36. R.J. Reynolds, L.M. Haffner, and S.L. Tufte, 1999, *ApJ*, 525, L21
37. R.-J. Dettmar, 2003, *Acta Astronomica Sinica*, Vol. 44 Suppl., 106
38. M.A. Brentjens, and A.G. de Bruyn, 2005, *Astron. Astrophys.*, 441, 1217
39. A.G. de Bruyn, and M.A. Brentjens, 2005, *Astron. Astrophys.*, 441, 931
40. B.J. Burn, 1966, *MNRAS*, 133, 67
41. E.N. Vinyajkin, and V.A. Razin, 2002, in 'Astrophysical Polarized Backgrounds', Eds. S. Cecchini et al., AIP 609, 26
42. A. Wilkinson, F.G. Smith, 1974, *MNRAS*, 167, 593

43. M. Wolleben, 2005, PhD-Thesis, Bonn University
44. P.M.W. Kalberla, U. Mebold, and W. Reich, 1980, *Astron. Astrophys.*, 82, 275
45. W.N. Brouw, and T.A.Th. Spoelstra, 1976, *Astron. Astrophys. Suppl.*, 26, 129
46. T.A.Th. Spoelstra, 1984, *Astron. Astrophys.*, 135, 238
47. M.H. Wieringa, A.G. de Bruyn, D. Jansen, W.N. Brouw, and P. Katgert, 1993, *Astron. Astrophys.*, 268, 215
48. M. Haverkorn, P. Katgert, and A.G. de Bruyn, 2000, *Astron. Astrophys.*, 356, L13
49. M. Haverkorn, P. Katgert, and A.G. de Bruyn, 2002, in 'Astrophysical Polarized Backgrounds', Eds. S. Cecchini et al., AIP 609, 72
50. M. Haverkorn, P. Katgert, and A.G. de Bruyn, 2003, *Astron. Astrophys.*, 403, 1031
51. M. Haverkorn, P. Katgert, and A.G. de Bruyn, 2003, *Astron. Astrophys.*, 403, 1045
52. M. Haverkorn, P. Katgert, and A.G. de Bruyn, 2003, *Astron. Astrophys.*, 404, 233
53. M. Haverkorn, P. Katgert, A.G. de Bruyn, and F. Heitsch, 2004, in 'The Magnetized Interstellar Medium', Eds. B. Uyaniker, W. Reich, R. Wielebinski, Copernicus GmbH, 81
54. M. Haverkorn, P. Katgert, and A.G. de Bruyn, 2004, *Astron. Astrophys.* 427, 549
55. M. Haverkorn, and F. Heitsch, 2004, *Astron. Astrophys.*, 421, 1011
56. M. Wolleben, T.L. Landecker, W. Reich, and R. Wielebinski, 2006, *Astron. Astrophys.*, in press
57. M. Wolleben, T.L. Landecker, W. Reich, and R. Wielebinski, 2004, in 'The Magnetized Interstellar Medium', Eds. B. Uyaniker, W. Reich, R. Wielebinski, Copernicus GmbH, 51
58. J.C. Testori, P. Reich, and W. Reich, 2004, in 'The Magnetized Interstellar Medium', Eds. B. Uyaniker, W. Reich, R. Wielebinski, Copernicus GmbH, 57
59. W. Reich, P. Reich, and E. Fürst, 1990, *Astron. Astrophys. Suppl.*, 83, 539
60. P. Reich, W. Reich, and E. Fürst, 1997, *Astron. Astrophys. Suppl.*, 126, 413
61. W. Reich, E. Fürst, C.G.T. Haslam, P. Steffen, and K. Reif, 1984, *Astron. Astrophys. Suppl.*, 58, 197

62. W. Reich, E. Fürst, P. Reich, and K. Reif, 1990, *Astron. Astrophys. Suppl.*, 85, 633
63. E. Fürst, W. Reich, P. Reich, and K. Reif, 1990, *Astron. Astrophys. Suppl.*, 85, 691
64. W.J. Altenhoff, D. Downes, T. Pauls, and J. Schraml, 1979, *Astron. Astrophys. Suppl.*, 35, 23
65. R.F. Haynes, J.L. Caswell, and L.W.J. Simons, 1978, *Aust. J. of Physics, Astrophysical Suppl.*, 45, 1
66. A.R. Duncan, R.T. Stewart, R.F. Haynes, and K.L. Jones, 1995, *MNRAS*, 277, 36
67. T. Handa, Y. Sofue, N. Nakai, H. Hirabayashi, and M. Inoue, 1987, *PASJ*, 39, 709
68. A.R. Taylor, S.J. Gibson, M. Peracaula, et al., 2003, *AJ*, 125, 3145
69. N. Junkes, E. Fürst, and W. Reich, 1987, *Astron. Astrophys. Suppl.*, 69, 451
70. A.R. Duncan, P. Reich, W. Reich, and E. Fürst, 1999, *Astron. Astrophys.*, 350, 447
71. A.R. Duncan, R.F. Haynes, K.L. Jones, and R.T. Stewart, 1997, *MNRAS*, 291, 279
72. W. Reich, E. Fürst, P. Reich, B. Uyaniker, R. Wielebinski, and M. Wolleben, 2004, in 'The Magnetized Interstellar Medium', Eds. B. Uyaniker, W. Reich, R. Wielebinski, Copernicus GmbH, 45
73. B. Uyaniker, E. Fürst, W. Reich, P. Reich, and R. Wielebinski, 1998, *Astron. Astrophys. Suppl.*, 132, 401
74. B. Uyaniker, E. Fürst, W. Reich, P. Reich, and R. Wielebinski, 1999, *Astron. Astrophys. Suppl.*, 138, 31
75. Z.Z. Abidin, J.P. Leahy, A. Wilkinson, P. Reich, W. Reich, and R. Wielebinski, 2003, *New Astronomy Review*, Vol.47, Issue 11-12, 1151
76. The GALFA Consortium, 2003, *Galactic Astronomy with the Arecibo L-band feed array (ALFA)* ([http://alfa.naic.edu/galactic/alfa\\_galactic.html](http://alfa.naic.edu/galactic/alfa_galactic.html))
77. B. Uyaniker, T.L. Landecker, A.D. Gray, and R. Kothes, 2003, *ApJ*, 585, 785
78. T.L. Landecker, B. Uyaniker, and R. Kothes, 2002, in 'Astrophysical Polarized Backgrounds', Eds. S. Cecchini et al., AIP 609, 9
79. R. Kothes, and T.L. Landecker, 2004, in 'The Magnetized Interstellar Medium', Eds. B. Uyaniker, W. Reich, R. Wielebinski, Copernicus GmbH, 33

80. R.I. Reid, 2004, in 'The Magnetized Interstellar Medium', Eds. B. Uyaniker, W. Reich, R. Wielebinski, Copernicus GmbH, 39
81. B.M. Gaensler, J.M. Dickey, N.M. McClure-Griffiths, A.J. Green, M.H. Wieringa, and R.F. Haynes, 2001, ApJ, 549, 959
82. M. Haverkorn, B.M. Gaensler, J.C. Brown, N.M. McClure-Griffiths, J.M. Dickey, and A.J. Green, 2005, astro-ph\0511407
83. X.H. Sun, W. Reich, J.L. Han, P. Reich, and R. Wielebinski, 2006, Astron. Astrophys., in press.
84. S. Rys, K.T. Chyzy, A. Kus, E. Pazderski, M. Soida, and M. Urbanik, 2006, AN, in press
85. W. Reich, E. Fürst, P. Reich, R. Wielebinski, and M. Wolleben, 2002, in 'Astrophysical Polarized Backgrounds', Eds. S. Cecchini et al., AIP 609, 3
86. R. Reid, 2005, CGPS News Vol. 33
87. D.D. Sokoloff, A.A. Bykov, A. Shukurov, E.M. Berkhuijsen, R. Beck, and A.D. Poezd, 1998, MNRAS, 299, 189
88. A.D. Gray, T.L. Landecker, P.E. Dewdney, A.R. Taylor, A.G. Willis, and M. Normandeau, 1999, ApJ, 514, 221
89. M. Wolleben, and W. Reich, 2004, in 'The Magnetized Interstellar Medium', Eds. B. Uyaniker, W. Reich, R. Wielebinski, Copernicus GmbH, 99
90. M. Wolleben, and W. Reich, 2004, Astron. Astrophys., 427, 537
91. R. Kothes, T.L. Landecker, M. Wolleben, T. Foster, and W. Reich, 2004, CGPS News, Vol. 31
92. B. Uyaniker, and T.L. Landecker, 2002, ApJ, 575, 225
93. B. Uyaniker, 2004, in 'The Magnetized Interstellar Medium', Eds. B. Uyaniker, W. Reich, R. Wielebinski, Copernicus GmbH, 71
94. E.N. Vinyajkin, 2004, in 'The Magnetized Interstellar Medium', Eds. B. Uyaniker, W. Reich, R. Wielebinski, Copernicus GmbH, 93
95. W. Reich, 2005, AN, 326, 620
96. J.D. Peterson, and W.R. Webber, 2002, ApJ, 575, 217
97. A. Shukurov, and E.M. Berkhuijsen, 2003, MNRAS, 342, 496
98. R. Beck, A. Shukurov, D. Sokoloff, and R. Wielebinski, 2003, Astron. Astrophys., 411, 99
99. J.C. Brown, A.R. Taylor, and B.J. Jackel, 2003, ApJS, 145, 213

100. R. Beck, and G.M. Gaensler, 2004, in 'Science with the Square Kilometre Array', Eds. C. Carilli, S. Rawlings, *New Astronomy Reviews*, 48, 1289
101. E.M. Berkhuijsen (Ed.), 1999, 'Galactic Foreground Polarization', Max-Planck-Institut für Radioastronomie
102. T.L. Landecker (Ed.), 2001, 'Radio Polarization: A New Probe of the Galaxy', DRAO Penticton
103. S. Cecchini, S. Cortiglioni, R. Sault, and C. Sbarra (Eds.), 2002, 'Astrophysical Polarized Backgrounds', AIP, Vol. 609
104. B. Uyaniker, W. Reich, and R. Wielebinski (Eds.), 2004, 'The Magnetized Interstellar Medium', Copernicus GmbH  
(<http://www.mpifr-bonn.mpg.de/div/konti/antalya/contrib.html>)
105. L. La Porta, and C. Burigana, 2006, *Astron. Astrophys.*, in press
106. C. Burigana, L. La Porta, P. Reich, and W. Reich, 2006, *Astron. Nachrichten*, in press
107. M. Tucci, E. Carretti, S. Cecchini, L. Nicastro, R. Fabbri, B.M. Gaensler, J.M. Dickey, and N.M. McClure-Griffiths, 2002, *ApJ*, 579, 607
108. M. Zaldarriaga, and U. Seljak, 1997, *Phys. Rev. D.*, 55, 1830
109. W.H. Kinney, 1998, *Phys. Rev. D.*, 58, 123506
110. E. Carretti, G. Bernardi, S. Cecchini, et al., 2002, in 'Experimental Cosmology at Millimetre Wavelength', Eds. M. De Petri, M. Gervasi, AIP 616, 140
111. S. Cortiglioni, et al., 2003, in '16th ESA Symposium on European Rocket and Balloon Programmes and Related Research', Ed. B. Warmbein, ESA Proc. SP-530, 271
112. E. Carretti, S. Poppi, W. Reich, P. Reich, E. Fürst, G. Bernardi, S. Cortiglioni, and C. Sbarra, 2006, *MNRAS*, in press